University of Tartu
Faculty of Science and Technology
Institute of Physics

Taavi Pungas

The microscopic magnetic model of Cu(OH)Cl

Master's Thesis

Supervisors:
Alexander A. Tsirlin
Taavi Vaikjärv

Approved for defence: .....

.....
(signature, date)

Tartu 2014

Contents

Abbreviations

DFT	**D**ensity **F**unctional **T**heory
DOS	**D**ensity **o**f **S**tates
ED	**E**xact **D**iagonalisation
GGA	**G**eneralised **G**radient **A**pproximation
HTSE	**H**igh **T**emperature **S**eries **E**xpansion
LDA	**L**ocal **D**ensity **A**pproximation

Physical constants and conventions

The following physical constants are often referred to in this work:

$N_A = 6.02214129(27) \cdot 10^{23}$ mol^{-1}	Avogadro constant
$\mu_B = 9.27400968(20) \cdot 10^{-24}$ J T^{-1}	Bohr magneton
$k_B = 1.3806488(13) \cdot 10^{-23}$ J K^{-1}	Boltzmann constant

In accordance with the customs of this field of science, some physical quantities are not reported in SI units. Magnetisation, normally an extensive quantity, is measured in μ_B per magnetic site, thus effectively giving the site's magnetic moment as a fraction of that of a free electron. Magnetic susceptibility is reported in emu/mol, i.e. in CGS electromagnetic units normalised per mole of particles instead of unit volume or mass of the compound.

Physical quantities with energy dimension are mostly reported in units of Kelvin. The conversion from the value of a quantity in Kelvin to that in Joules can be made by multiplying with k_B. The use of this convention makes clear the temperature scale where energy of thermal fluctuations becomes comparable with the energy of the described phenomenon.

1. Introduction

Low-dimensional magnetism, especially in Cu^{2+} compounds, has proved itself to be a surprisingly diverse field of study. Mainly concerned with investigating the magnetic properties of compounds and relevant models with chains or layers of spins, it has contributed to the emergence of many interesting physical phenomena. Arguably the most intriguing of those is the high-T_c superconductivity in layered cuprates with CuO_2 planes [1]. As claimed by Anderson [2], it is closely related to the existence of new phases of the 2D spin-$\frac{1}{2}$ Heisenberg model, favoured by low spin, low dimensionality, and magnetic frustration.

An example more specific to low-dimensional magnetism is the spin-Peierls transition, where a uniform antiferromagnetic chain undergoes dimerisation into a system with a non-magnetic spin singlet ground state [3]. Although first observed in an organic compound [4], it was soon also discovered in a Cu^{2+} material $CuGeO_3$ [5]. Bose-Einstein condensation, in contrast, is a fundamental phenomenon well known in other branches of physics, but it also appears naturally in magnetic systems. Magnons, elementary excitations in antiferromagnets, have been found to condense in a number of magnetic materials with even richer physics than in canonical Bose-Einstein condensates [6].

The phenomena described above are extreme examples of what kind of physics can be found in magnetic materials when they are investigated in detail. In other cases, one might not need a better description of a compound than whether it is para- or diamagnetic. However, it is possible that when looked into, a seemingly ordinary material displays some new feature or allows us to gain insight into some previously known model. The latter is often the main motivation behind studying

a new compound from the perspective of microscopic magnetic modelling. And if the system is found to have interesting features, further experimental work can be launched to investigate the details. Not less importantly, microscopic magnetic modelling studies also enhance our understanding of the nature of microscopic magnetic interactions in the diverse crystal structures and chemistries of inorganic materials.

The aim of this thesis is to establish the microscopic magnetic model of Cu(OH)Cl by means of *ab-initio* calculations and refine the model parameters by fitting experimental data with simulated curves. It is proposed that the magnetic properties of the material are best explained by a quasi-two-dimensional spin-$\frac{1}{2}$ antiferromagnetic Shastry-Sutherland model. Because of its strongly frustrated nature, the Shastry-Sutherland model [7] has several zero-temperature ground states in different parameter regions. There has been much discussion about the characteristics of these quantum phases and phase transitions [8], but so far experimental evidence has been scarce. This makes the discovery of a new Shastry-Sutherland compound especially significant – Cu(OH)Cl provides an opportunity for further studies into the model and its properties.

This thesis is structured in the following way. Chapter 2 gives an overview of magnetism on a microscopic level, explaining the mechanisms of interaction between localised magnetic moments in crystals and how to model them. Description and initial analysis of the structure and experimental characteristics of Cu(OH)Cl follows, together with details about the Shastry-Sutherland model. Then, methods that were used to carry out this work are explained, after which we give an account of our results. Finally, the results are discussed and conclusions are drawn.

2. Overview of magnetism on a microscopic level

2.1 A microscopic view on magnetic interactions

From everyday experience it might seem that ferromagnetism is the only magnetic phenomenon occurring in materials. This is of course not the case, but it is true that other magnetic phenomena in materials have weaker effects on the surroundings. All magnetic phenomena share one principal property, though: they have their origin on the microscopic scale, and one has to investigate them on the microscopic level to gain any insights.

The first and most important requirement for observing magnetic phenomena in a system is that it needs to contain unpaired electrons. Still, the mechanism how magnetism arises depends very much on whether these unpaired electrons are delocalised over the whole system (like in metals) or localised on specific sites (mostly in insulators). As this work is focused on Cu(OH)Cl, an insulator with localised unpaired electrons, only the mechanisms relevant for the latter case are considered here.

Magnetism is inherently a quantum effect, arising from strong correlations between electrons as prescribed by the many-body wavefunction. In macroscopic systems, a full quantum mechanical treatment based on the many-body Schrödinger equation is impossible, meaning that approximate models need to be used to make progress. A useful simplification is considering only pairwise correlations, thus neglecting the

possibility of three-body (etc.) interactions. The Heisenberg model [9] uses exactly this approach, describing a collection of spins with the Hamiltonian

$$\hat{H} = \sum_i \sum_{j<i} J_{ij} \hat{\boldsymbol{S}}_{\boldsymbol{i}} \cdot \hat{\boldsymbol{S}}_{\boldsymbol{j}} \tag{2.1}$$

Here, J_{ij} denotes the exchange coupling between the pair of spins on sites i and j, the full Hamiltonian forms as a sum over all pairs of interactions. The maximum possible expectation value of $\hat{\boldsymbol{S}}_{\boldsymbol{i}} \cdot \hat{\boldsymbol{S}}_{\boldsymbol{j}}$ is $\frac{1}{4}$ (for a spin triplet) and minimum $-\frac{3}{4}$ (for a spin singlet) – here we absorb $\hbar^2$ into J_{ij} to make the spin operators dimensionless. A positive J_{ij} means that the spin singlet configuration lies lower in energy and the interaction is antiferromagnetic, forcing the spins to oppose one another. Conversely, in case of a negative J_{ij} the spin triplet configuration has lower energy and the interaction is ferromagnetic, favouring parallel spins. We also see that J_{ij} is the energy difference between the ferromagnetic and antiferromagnetic configurations.

The Heisenberg model provides a very convenient description of interacting magnetic sites on a lattice, because it is independent of the particular mechanism that gives rise to the exchange couplings and simply assigns spins to localised sites. There is a number of pathways how exchange couplings can emerge, and of course they require describing the system on the level of electrons and orbitals. The simplest of these is direct exchange, in which electrons on neighbouring magnetic atoms directly interact with one another [10]. In that case, the lowest-energy configuration is the spatially symmetric bonding orbital and it will be occupied by a pair of electrons. Since the overall wavefunction of the system has to be antisymmetric under the exchange of the two electrons, having a symmetric spatial part of the wavefunction means that the spin part must be antisymmetric (a singlet), thus resulting in an antiferromagnetic interaction. However, in real crystals neighbouring magnetic ions are usually too far apart to have a significant overlap between the wavefunctions of their unpaired electrons [10]. This means that in most cases, direct exchange cannot explain the presence of antiferromagnetic exchange couplings and alternative mechanisms have to be considered.

The most common way how exchange couplings arise in ionic solids is a mechanism called superexchange or Kramers-Anderson exchange [11, 12]. It requires that the half-filled d-orbitals of the two interacting magnetic ions overlap with the same filled p-orbital of an intermediate ion. This is often the case in oxides and halogenides (e.g. Cu(OH)Cl), where magnetic ions are usually separated by ligands with a filled p-shell.

The Hubbard model [13] gives us a framework in which to describe superexchange. It is one of the simplest approximate models in solid-state physics, describing interacting particles on a lattice by using only two terms in the Hamiltonian:

$$\hat{H} = -\sum_{i}\sum_{j<i}\sum_{\sigma} t_{ij}(\hat{c}^{\dagger}_{i,\sigma}\hat{c}_{j,\sigma} + \hat{c}^{\dagger}_{j,\sigma}\hat{c}_{i,\sigma}) + U_{\text{eff}}\sum_{i}\hat{n}_{i\uparrow}\hat{n}_{i\downarrow} \tag{2.2}$$

Here, σ denotes the spin projection ($\uparrow$ or $\downarrow$). $\hat{c}^{\dagger}_{i,\sigma}$ and $\hat{c}_{i,\sigma}$ are the creation and annihilation operators of spin-σ particles on site i, making $\hat{n}_{i\sigma} = \hat{c}^{\dagger}_{i\sigma}\hat{c}_{i\sigma}$ the corresponding particle number operator. The first term describes the kinetic energy of the particles, it allows electrons to jump from one site to another. The strength of the interaction between two sites is described by the hopping parameter t_{ij}. The second term assigns the energy penalty U_{eff} for having two particles on the same site – without it, the formula reduces to the simple tight-binding model.

In the strongly correlated regime where interactions between sites are weak ($t_{ij} \ll U_{\text{eff}}$), it can be shown by perturbation theory that the Hubbard model leads to Heisenberg exchange couplings $J_{ij} = 4t_{ij}^2/U_{\text{eff}}$ [14], which are always antiferromagnetic. The effect can be understood by thinking of the hopping term as allowing antiferromagnetically oriented spins to be delocalised over neighbouring sites (albeit at the energy cost U_{eff}), thus reducing their kinetic energy. If the two spins are parallel, this delocalisation is not possible – by the Pauli principle, two electrons with the same spin are not allowed to occupy the same site, hence intersite hoppings are forbidden. As a result, if the structure of a compound shows that two magnetic ions are linked by an oxygen atom, we expect superexchange to give rise to an antiferromagnetic exchange coupling between them.

However, this does not mean that only antiferromagnetic couplings can occur between localised magnetic moments. If the angle between the magnetic site - ligand bonds is around 90°, then the half-filled d-shells of magnetic ions only overlap very little with the same p-orbital and superexchange is not the dominant interaction mechanism. By using $LiCu_2O_2$ as an example compound, it has been shown that a ferromagnetic interaction dominates in the case of a near-90° Cu-O-Cu angle. This ferromagnetic interaction has been attributed to Hund's coupling on the ligand site, because DFT calculations indicate substantial mixing between Cu and O orbitals [15]. Intuitively, this can be understood in terms of a second-order process in which two Cu^{2+} sites receive an electron from two filled p-orbitals of the same oxygen ion. If the spins on the Cu sites are initially parallel, the oxygen ion is left with two parallel unpaired electrons on its p-orbitals. Conversely, if the Cu spins are initially antiparallel, there will be two electrons with antiparallel spins on the oxygen p-orbitals. Due to Hund's coupling between the two unpaired electrons on the oxygen, the former configuration is favoured over the latter one and a ferromagnetic interaction is observed.

The Heisenberg model does not capture all possible magnetic interactions that can occur between localised magnetic moments. Quite commonly, Dzyaloshinsky–Moriya (DM) interactions [16, 17] need to be added to the Heisenberg model to account for all details of the real magnetic behaviour. The form of Eq. (1) implies that the magnetic response does not depend on the direction of the applied field, which is rarely the case experimentally. Also known as the anisotropic exchange interaction, if present between sites i and j it introduces to the Hamiltonian the term

$$\hat{H}_{ij} = \boldsymbol{D_{ij}} \cdot \hat{\boldsymbol{S}}_{\boldsymbol{i}} \times \hat{\boldsymbol{S}}_{\boldsymbol{j}}. \tag{2.3}$$

The DM interaction has been found to be the leading source of anisotropy in cuprates [14]. It arises if spin-orbit interaction is considered on top of superexchange, and as such a correction it has a much smaller magnitude than the main Heisenberg exchange coupling, $|\boldsymbol{D_{ij}}| \ll J_{ij}$. Since the effect of the DM interaction is to cant the spins slightly, it is sometimes noticed as a small ferromagnetic correction to a normally antiferromagnetic system.

Due to the mechanism underlying the origin of DM interactions, it can only arise between two sites if the crystal does not have inversion symmetry with respect to the centre of the line connecting the two magnetic ions [17]. Therefore it is possible to tell whether an exchange coupling can be influenced by DM corrections just by inspecting the crystal structure of the compound.

The brief description of magnetic interactions that has been presented so far is of course incomplete and remains restricted to insulators. However, due to the many-body nature of condensed matter phenomena and the tight connection between magnetism and strong electronic correlations, no such complete description exists. The only way to figure out a detailed microscopic model of an actual compound is by undertaking a comprehensive study combining its experimental properties and simulation results.

2.2 Low-dimensional magnetism in Cu^{2+} compounds

The Cu^{2+} ion with its $[Ar]3d^9$ electron configuration contains an unpaired electron and thus is magnetic. Furthermore, as it is only one electron short of having a filled d-shell, the ion has a fixed total spin $S = \frac{1}{2}$. This is the simplest possible case for microscopic modelling, and it means that systems with Cu^{2+}-based magnetism can be modelled with better precision than most others.

Another benefit of studying Cu^{2+} compounds is the (near) lack of spin-orbit coupling when compared with heavier elements, meaning that its spin is not mixed with orbital angular momentum considerably. This is seen most clearly from the experimentally observed magnetic moments of Cu^{2+} ions in various compounds. The magnetic moment of a spin-$\frac{1}{2}$ particle can be expressed as $\mu = \frac{1}{2} g \mu_B$, with g the g-factor. The absolute value of a free electron's g-factor is 2.002319 and in most low-dimensional Cu^{2+} compounds it is found to be close to that, often around $2.15 \ldots 2.20$ [18, 19]. Given that the g-factors of some heavy $S = \frac{1}{2}$ ions

easily exceed the free electron value by a factor of two or more (e.g. $g = 5.43$ in the model compound Yb_2Pt_2Pb [20]), we see the values for Cu^{2+} ions are very close to the free electron one. Due to the weakness of spin-orbit coupling in Cu^{2+} compounds, their magnetic properties are almost independent of the direction of the applied magnetic field, i.e. have very low anisotropy.

Many examples of low-dimensional $S = \frac{1}{2}$ magnetism have been discovered in Cu^{2+} compounds. Cu^{2+} ions are often found in CuX_4 plaquettes, where each copper ion is surrounded by four anions X, with X = O, F, Cl, etc. These plaquettes in turn can be arranged in various configurations, most often forming chains or layers of some sort and resulting in low-dimensional interaction topologies (see Figure 2.1). Examples of one-dimensional magnetism in Cu^{2+} compounds include straightforward microscopic magnetic models like ferromagnetic and antiferromagnetic chains, a nearly ideal realisation of the latter which was found in $KCuF_3$ [21]. More interesting 1D configurations also exist, e.g. two- and three-leg antiferromagnetic spin ladders in $SrCu_2O_3$ and $Sr_2Cu_3O_5$, respectively [22]. Two-dimensional examples are even more numerous. Two of the more noteworthy and exotic configurations that have been observed in Cu^{2+} compounds are the kagome lattice (in $ZnCu_3(OH)_6Cl_2$, known for its quantum spin liquid state [23]) and the Shastry-Sutherland lattice (in $SrCu_2(BO_3)_2$ [24]).

Some of the models in Figure 2.1 display a phenomenon called geometrical frustration, meaning that the geometry of the lattice introduces conflicting exchange couplings between sites. Strongly frustrated models have sparked much interest in physics, since frustration often gives rise to complex effects in the system. Strong frustration can lead to a multitude of ground states even at zero temperature. As another consequence, frustration shifts the onset of magnetic ordering to much lower temperatures than would otherwise be expected. Examples of strongly frustrated systems include the triangular lattice, the kagome lattice and the Shastry-Sutherland lattice (Figure 2.1).

It has been proved rigorously that at any finite temperature, no one- or two-dimensional isotropic Heisenberg spin model with finite-range exchange interaction

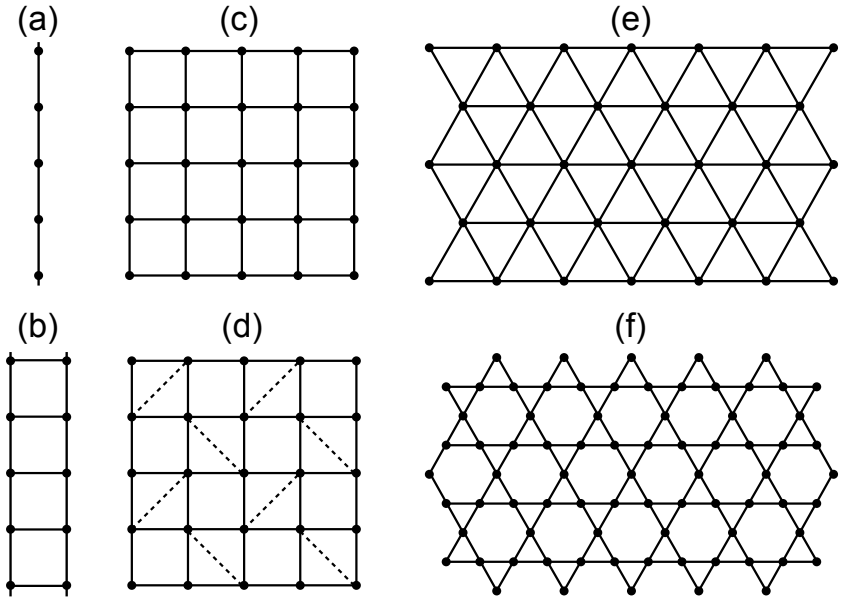

FIGURE 2.1: Examples of lattices encountered in microscopic magnetic modelling: (a) chain, (b) ladder, (c) square lattice, (d) Shastry-Sutherland lattice, (e) triangular lattice, (f) kagome lattice. Of these examples, (d)-(f) are geometrically frustrated.

can undergo long-range magnetic ordering [25]. Despite that, magnetic ordering is commonly seen even in the compounds that are characterised by low-dimensional microscopic magnetic models. This apparent contradiction arises from the fact that none of the real-world materials are really one- or two-dimensional, there always exist additional couplings that link the chains or layers together into a three-dimensional structure. These interchain/interlayer couplings can be very weak, but in no case are they identically zero. Also, it turns out that even though the magnetic ordering temperature depends on the magnitude of the interchain/interlayer coupling, already a very weak coupling is sufficient to shift the ordering temperature to moderate values. It has been shown that in case of the spin-$\frac{1}{2}$ antiferromagnetic square lattice with intralayer coupling J, interlayer couplings over $0.001J$ already give rise to Néel ordering above temperature $0.25J$ [26]. Of course, in a frustrated system the effect will be much less pronounced, but still we expect magnetic ordering to take place at a reasonable temperature. As a result, when a compound is said to display e.g. two-dimensional magnetism, in reality it is quasi-two-dimensional and can show signatures of magnetic ordering, albeit at very low temperatures.

3. Analysis of previous results on Cu(OH)Cl

3.1 Crystal structure of Cu(OH)Cl

By X-ray diffraction studies, Cu(OH)Cl has been found to crystallise in space group $P2_1/c$ and thus to belong in the monoclinic crystal system [27]. Its unit cell parameters are outlined in Table 3.1.

TABLE 3.1: Unit cell parameters of Cu(OH)Cl.

Lengths (Å)		Angles	
a	6.2953(4)	α	90°
b	6.6649(11)	β	118.138(11)°
c	5.5580(4)	γ	90°

Due to the low atomic number of hydrogen (meaning low electron density at H atoms), experimentally determined positions of hydrogen atoms are subject to large uncertainty. In fact, it has been shown that using imprecise values of hydrogen positions can lead to physically unsound results in microscopic magnetic modelling [28]. Therefore before a detailed analysis of magnetic interactions in a compound, hydrogen positions must often be refined. In case of Cu(OH)Cl, the need for that is clear: the experimentally determined structure [27] has O-H bond length 1.3 Å instead of the usual 1.0 [28]. To solve the problem, the hydrogen position was allowed to relax in a series of LDA calculations for geometry optimisation – a method that has been shown to be a viable alternative to elaborate experiments [29]. This way the expected O-H bond length 1.0 Å was obtained

(for computational details, see Section 4.1.2). All subsequent calculations and discussions in this work are based on this hydrogen-relaxed crystal structure, the Wyckoff positions of which are given in Table 3.2.

TABLE 3.2: Wyckoff positions (in fractional coordinates) of atoms in the experimental (H^{exp}) and hydrogen-relaxed (H^{rel}) structures. Upon relaxation, the O-H bond length decreased from 1.3 Å to 1.0 Å.

Atom	x/a	y/b	z/c
Cu	0.03201(7)	0.11772(6)	0.28577(7)
Cl	0.3115(1)	0.0907(1)	0.1334(2)
O	0.8807(4)	0.1478(3)	0.5318(5)
H^{exp}	0.674(14)	0.128(8)	0.528(12)
H^{rel}	0.7006	0.1635	0.4309

The crystal structure of Cu(OH)Cl has been visualised in Figures 3.1 and 3.2. Figure 3.1 illustrates how Cu(OH)Cl consists of layers running along *bc*-planes. Neighbouring layers are held together by hydrogen bonds between the O-H group of one layer and Cl ion of the next.

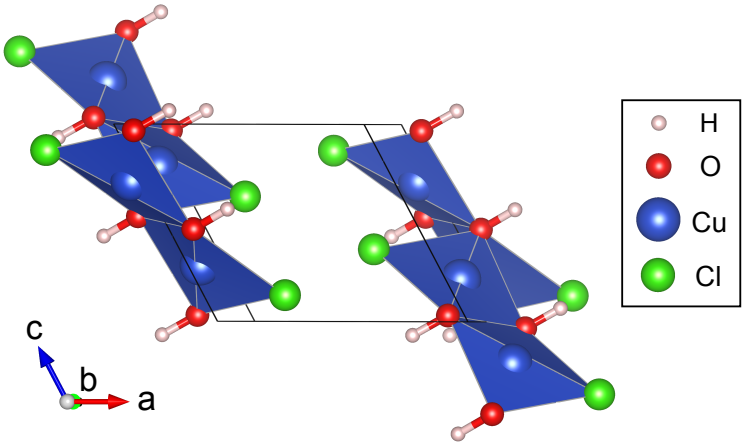

FIGURE 3.1: The crystal structure of Cu(OH)Cl. Layers of dimers run along bc-planes.

In Figure 3.2, a single layer is shown in more detail (hydrogen atoms have been omitted for clarity). Each Cu ion is surrounded by one chlorine and three oxygen atoms, constituting a $CuClO_3$ plaquette. Pairs of edge-sharing plaquettes form

dimers, and additionally each plaquette shares a corner (an oxygen ion) with four others.

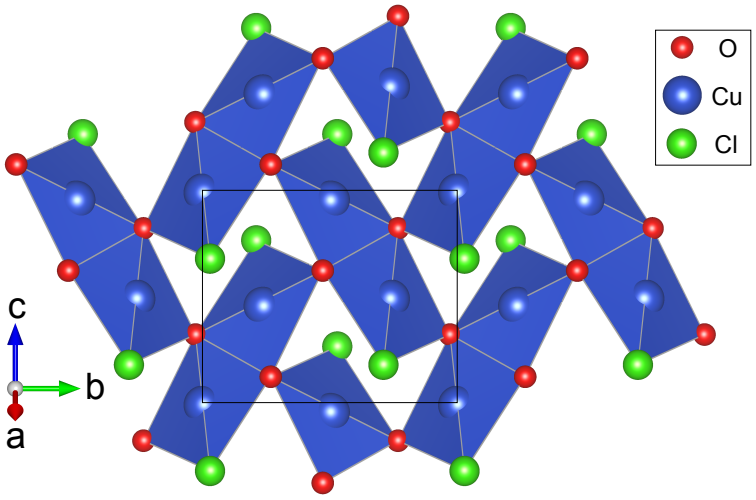

FIGURE 3.2: A single layer of Cu(OH)Cl, composed of dimers of $CuClO_3$ plaquettes. Each plaquette shares an oxygen corner with five others, thus presumably giving rise to exchange couplings. The unit cell is outlined with a rectangle. For clarity, H atoms have been omitted.

Because of the layered structure of Cu(OH)Cl, it can be expected to display quasi-two-dimensional magnetism, with much stronger exchange couplings within the layers than between them. There should be a sizeable antiferromagnetic exchange coupling between each pair of neighbouring Cu^{2+} ions that are linked by an oxygen ion, arising via the superexchange mechanism (as explained in Section 2.1). In the case of a layer of Cu(OH)Cl, this reasoning leads us to consider the Shastry-Sutherland lattice as a possible model.

3.2 The Shastry-Sutherland model

The crystal structure and $S = \frac{1}{2}$ nature of Cu(OH)Cl suggest that its magnetic properties could be described by the Heisenberg model on the Shastry-Sutherland lattice, first proposed and analysed in 1981 [7]. The Shastry-Sutherland lattice (Figure 3.3) is a square lattice of couplings J' with some extra diagonal bonds

J that introduce frustration to the system. However, what makes this particular model interesting is that it resorts very well to theoretical analysis – in the parameter range $J'/J \ll 1$, the system has a simple exact ground state.

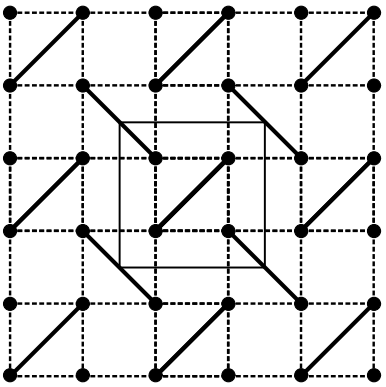

FIGURE 3.3: The Shastry-Sutherland lattice. J' couplings form a square lattice (broken lines) with some extra diagonal J couplings (solid lines). The unit cell of the lattice (thin-line square) contains four sites.

In Cu(OH)Cl, couplings within dimers of copper plaquettes correspond to J of the Shastry-Sutherland model. In addition to being part of a dimer, each copper plaquette shares a corner with two others, giving rise to interdimer couplings J'. It must be noted that in Cu(OH)Cl, these two plaquettes with which a corner is shared are not equivalent by symmetry, meaning that in principle there are two different interdimer couplings – we will denote these by J'_1 and J'_2. However, whether the two have the same magnitude or not cannot be determined by inspection, therefore further discussion has to be postponed until Chapter 5.

The first real-world example of the Shastry-Sutherland model was discovered in 1999 when magnetic properties of $SrCu_2(BO_3)_2$ were investigated [24]. It became the first compound with a spin system that could be described by the Heisenberg model on the Shastry-Sutherland lattice. In Figure 3.4, a schematic of the structure and exchange couplings of $SrCu_2(BO_3)_2$ is given. Even though the geometry looks different from that of the Shastry-Sutherland lattice, the two are topologically equivalent.

Since the discovery of $SrCu_2(BO_3)_2$, the Shastry-Sutherland model has drawn considerable attention. The main reason for that interest was the discovery of plateaux in the magnetisation curve of $SrCu_2(BO_3)_2$ corresponding to $\frac{1}{4}$ and $\frac{1}{8}$ of

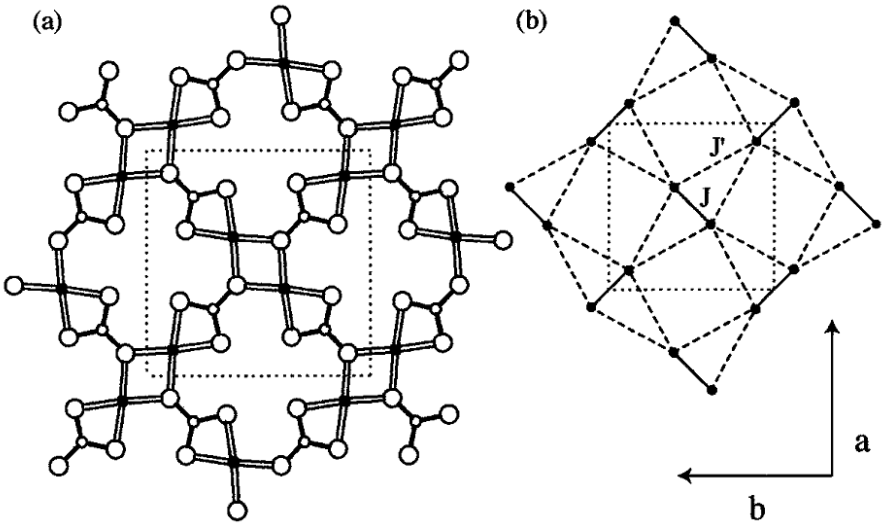

FIGURE 3.4: A schematic of the structure (a) and exchange couplings (b) of $SrCu_2(BO_3)_2$. Cu^{2+}, B^{3+} and O^{2-} ions are denoted by filled circles, small open circles and large open circles, respectively. The arrangement of exchange couplings is topologically equivalent to the Shastry-Sutherland lattice. Figure from Ref. [24].

the saturation moment [24], the first time when quantised magnetisation plateaux were observed in a 2D system. By now, the magnetisation curve of $SrCu_2(BO_3)_2$ has been measured up to 109 K and plateaux at $\frac{1}{3}$ and $\frac{1}{2}$ of the saturation moment have been detected [30, 31]. Using various simulation methods, the emergence of magnetic plateaux has also been thoroughly investigated theoretically, and spin structures at plateaux have been predicted. Intriguingly, translational symmetry of the lattice is spontaneously broken at the plateaux (except for the one at $\frac{1}{2}$ of the saturation moment) [8].

After $SrCu_2(BO_3)_2$, several other compounds with the Shastry-Sutherland lattice have been found, but so far none of those has been directly comparable with $SrCu_2(BO_3)_2$. For $(CuCl)LaNb_2O_7$, a spin-$\frac{1}{2}$ Shastry-Sutherland lattice has been proposed, with ferromagnetic (and different) couplings J_1' and J_2' [32]. A few classes of compounds have been discovered that contain rare-earth ions arranged in a Shastry-Sutherland lattice: Ln_2BaPdO_5 (Ln = La, Pr, Nd, Sm, Eu, Gd, Dy, Ho) [33], rare-earth tetraborides RB_4 (R = Tm, Tb, Dy, Ho, etc.) [34, 35], and metallic compounds Yb_2Pt_2Pb, Ce_2Pt_2Pb, Ce_2Ge_2Mg [20, 36].

In all these cases, for various reasons the physics tends to be only loosely related to

the original Shastry-Sutherland model with spin-$\frac{1}{2}$ isotropic Heisenberg couplings. One problem with rare earth ions is that spin-orbit coupling is strong enough to have a noticeable effect and produce a substantial anisotropy (e.g. presence of an easy axis), which makes magnetic properties of the system dependent on the orientation of the crystal with respect to the direction of the applied magnetic field. In these cases, the Ising model is often more appropriate than the Heisenberg model [37]. In metallic compounds, additional complications arise from Ruderman-Kittel-Kasuya-Yosida (RKKY) interactions, which are generally long-range and not restricted to J and J' [38–40]. Finally, most of the mentioned rare earth ions have $S > \frac{1}{2}$, meaning that the nice properties of the Shastry-Sutherland model concerning the formation of dimer singlets and triplet excitations are lost. Still, magnetisation plateaux have been observed in some of these compounds [34–36].

The properties of the Shastry-Sutherland model depend heavily on the ratio J'/J. Due to the lack of experimentally available compounds that would follow closely the $S = \frac{1}{2}$ Shastry-Sutherland model (other than $SrCu_2(BO_3)_2$), the work on this dependence has so far been theoretical. The main point of interest has been the quantum phase diagram of the Shastry-Sutherland model. Because of the extreme frustration present in the lattice, performing accurate simulations has been extremely challenging – over time, the problem has been approached with the help of many different methods [41–45].

Even though full analysis of the J'/J phase diagram is complicated, the extreme cases can be understood relatively easily [7]. For $J'/J \ll 1$, the system consists of (nearly) isolated dimers, leading to the exact dimer singlet ground state. This is called the dimer phase, there is a spin gap (i.e. a gap in the spectrum of magnetic excitations) and no long-range order. In contrast, for $J'/J \gg 1$, the system reduces to a 2D square lattice Heisenberg model, the ground state of which has long-range antiferromagnetic order and no spin gap (the Néel phase) [46].

The most interesting question concerns the intermediate region between the dimer phase and the Néel phase. Early studies suggested that there might be an additional intermediate phase, but initially there was some confusion about its exact

nature [8]. The overwhelming majority of more recent simulations agree that there is a plaquette phase with short-range order around $J'/J = 0.7$ [42, 43], not a columnar-dimer phase [44] or a helical phase [45], as alternatively proposed. State-of-the-art infinite projected entangled-pair states (iPEPS) simulations put the intermediate plaquette phase in the range $0.675(2) < J'/J < 0.765(15)$ [43]. The phase diagram of the Shastry-Sutherland model as determined by iPEPS simulations is given in Figure 3.5.

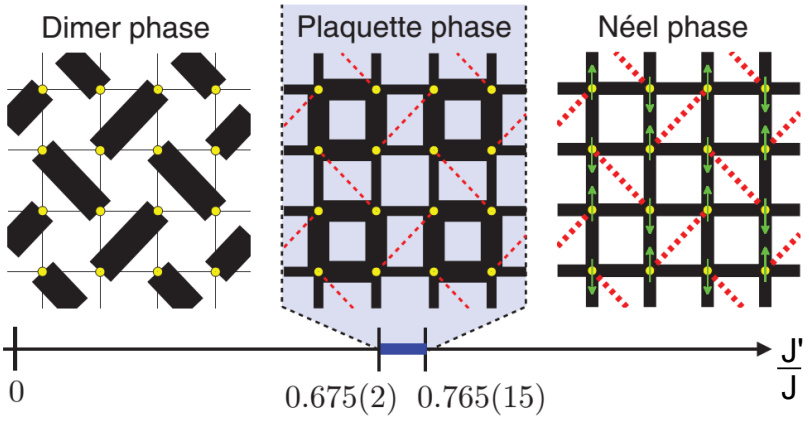

FIGURE 3.5: Phase diagram of the Shastry-Sutherland model as a function of J'/J. The width of a bond is proportional to the magnitude of the bond energy. Full lines correspond to positive energies and dashed lines to negative. The arrows in the right panel illustrate the Néel order. Figure from Ref. [43].

Clearly, there is a wealth of interesting physical phenomena linked to the Shastry-Sutherland lattice. Combined with the lack of well-behaved real-world examples, there is a strong incentive to look into the magnetic properties of Cu(OH)Cl more thoroughly. If confirmed as a Shastry-Sutherland compound, it would give a rare opportunity to investigate the details of the model and validate or refute theoretical predictions.

3.3 Experimental properties of Cu(OH)Cl

Magnetic susceptibility, magnetisation and heat capacity measurements have been performed on powder samples of Cu(OH)Cl, each of these physical properties can display features relevant to the microscopic magnetic model. Some qualitative

information may be extracted from the experimental curves simply by inspection and used to guide further modelling. However, details like exactly which model is most suitable and the numerical values of its parameters can only be deduced after theoretical simulations and fitting the data.

3.3.1 Magnetic susceptibility

The Curie law [47] predicts the molar magnetic susceptibility of a collection of isolated magnetic moments with spin angular momentum quantum number S to be

$$\chi = \frac{N_A g^2 \mu_B^2 S(S+1)}{3k_B T}. \tag{3.1}$$

The g-factor of a free electron is $g \approx 2.002319$, but due to spin-orbit coupling its value in a real compound is different and has to be fitted from experiment. In the presence of exchange couplings between magnetic moments, the temperature dependence of the Curie law is modified from $\chi \propto T^{-1}$ to $\chi \propto (T+\theta)^{-1}$ (the Curie-Weiss law [48]). If we also take into account that for an electron $S = \frac{1}{2}$, we obtain the final expression for magnetic susceptibility that is used to fit experimental data:

$$\chi = \frac{N_A g^2 \mu_B^2}{4k_B} \frac{1}{T+\theta}. \tag{3.2}$$

The theta-temperature θ is negative for ferromagnetic compounds. In case of positive values of θ, we have a compound in which antiferromagnetic exchange couplings are prevalent.

The magnetic susceptibility of Cu(OH)Cl was measured with Quantum Design MPMS SQUID magnetometer in the temperature range 2 – 380 K in various applied magnetic fields up to 5 T. According to the manufacturer, the sensitivity of magnetic moment measurements is $< 10^{-7}$ emu, which is less than 0.01% of our measured values (mostly above 10^{-3} emu). Therefore the main source of uncertainty for our experimental susceptibility and magnetisation curves is the possible presence of impurities in the sample, which may lead to systematic errors. Figure 3.6 shows the data collected in two different applied fields. There is only a

minor difference, which can be attributed to trace amounts of a ferromagnetic impurity. The curve obtained for highest applied magnetic field (i.e. 5 T) was used for detailed analysis and fitting, as it is least influenced by the presence of ferromagnetic impurities.

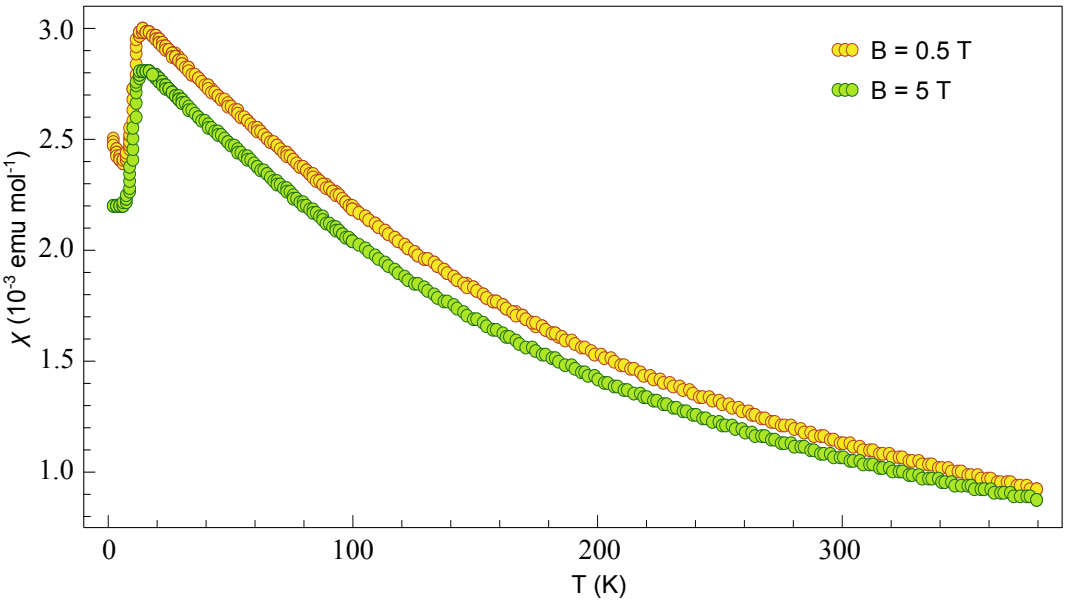

FIGURE 3.6: Experimental magnetic susceptibility curves of Cu(OH)Cl, measured at $B = 5$ T and $B = 0.5$ T. The susceptibility maximum is very compressed, probably due to strong frustration.

In general, the magnetic susceptibility curve behaves like expected for a material with prevalently antiferromagnetic exchange couplings. The high-temperature part of magnetic susceptibility curve follows the Curie-Weiss law, as can be best seen from the fact that its inverse is linear at high T (Figure 3.7). As temperature is lowered, the curve starts deviating from the Curie-Weiss law due to short-range magnetic ordering. Antiferromagnetic interactions (that were dominated by thermal motion at higher temperatures) start influencing spins noticeably and decrease the total magnetic moment of the crystal. As a result, a broad maximum of magnetic susceptibility occurs. Curiously, for Cu(OH)Cl the maximum is very compressed in comparison with what we observe in many other Cu^{2+} compounds [22, 28, 29, 49, 50]. This might be interpreted as an effect of the strong geometrical frustration of exchange couplings in the Shastry-Sutherland lattice.

The susceptibility curve gave a good Curie-Weiss fit above 250 K (Figure 3.7) and resulted in the theta-temperature $\theta = 80$ K with $g = 2.07$. The fact that we

obtained a g-factor close to 2 confirms that spin-orbit coupling is relatively weak. And as expected, θ is positive since antiferromagnetic couplings dominate between magnetic moments in Cu(OH)Cl. The theta-temperature is related to the values of exchange couplings in the following way [51]:

$$\theta = \frac{S(S+1)}{3} \sum_j J_{ij} = \frac{1}{4} \sum_j J_{ij}. \tag{3.3}$$

In other words, θ is (a quarter of) the sum of all exchange couplings affecting a magnetic site. The usefulness of this relation becomes evident in Section 5.1.3 – it presents a very straightforward way how to compare *ab-initio* values of exchange couplings with experiment.

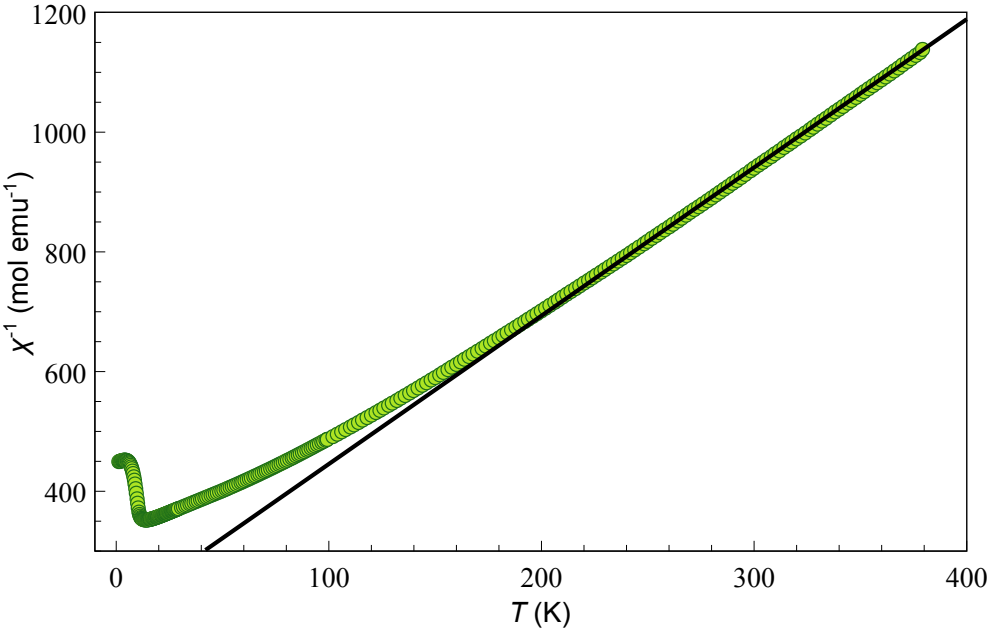

FIGURE 3.7: Inverse magnetic susceptibility with its Curie-Weiss fit above 250 K, giving the theta-temperature $\theta = 80$ K with $g = 2.07$.

Upon investigating the low-temperature region of magnetic susceptibility more closely (Figure 3.8), we find that in addition to the broad maximum there is an anomaly that can be associated with a phase transition, namely the slope changes abruptly at 11 K. However, this feature of the susceptibility curve is smeared out in practice, which is why a peak in the magnetic heat capacity is usually sought for to identify a phase transition. Luckily, it has been shown by a rather general theoretical argument that variation of the magnetic specific heat

of a simple antiferromagnet should be very close to the behaviour the function $d(\chi T)/dT$, especially in the region near the transition to the Néel phase [52]. As shown in Figure 3.8, there is a clear peak in $d(\chi T)/dT$, indicating a phase transition at 11 K. This suggests that Cu(OH)Cl could be in the Néel part of the phase diagram of the Shastry-Sutherland model.

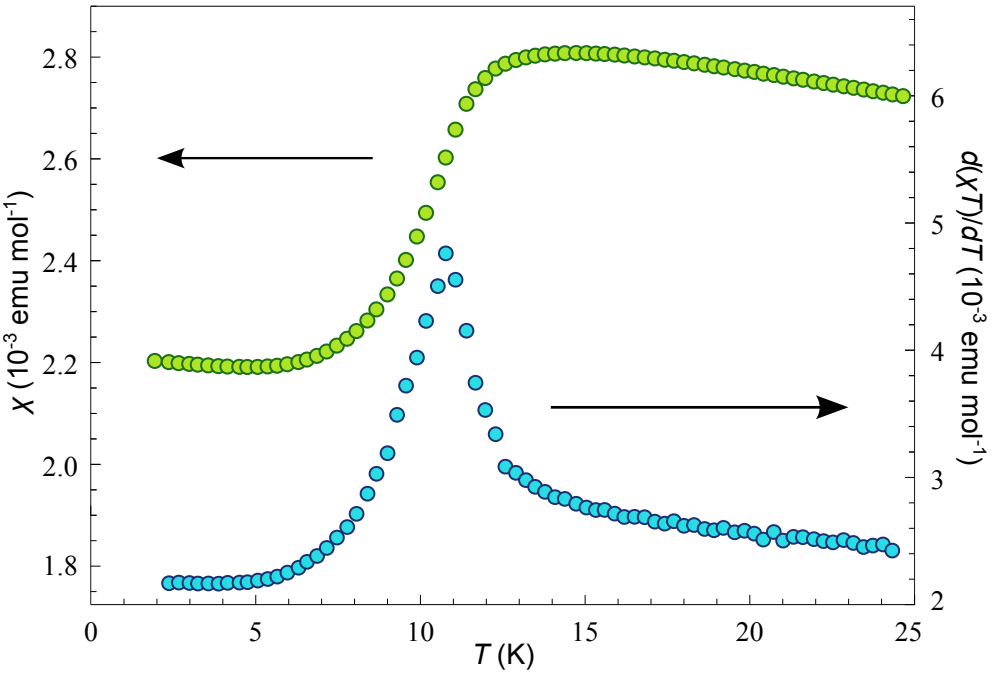

FIGURE 3.8: Low-temperature magnetic susceptibility results. The curve $\chi(T)$ has an abrubt change of slope at 11 K, whereas $d(\chi T)/dT$ displays a clear peak at 11 K. The behaviour of this function should closely resemble that of the magnetic heat capacity.

3.3.2 Magnetisation isotherm

The magnetisation curve was obtained for Cu(OH)Cl as a combination of two measurements. First, a magnetisation isotherm at $T = 2$ K was measured with Quantum Design MPMS SQUID magnetometer up to 5 T. Because of the difficulty of sustaining higher magnetic fields for extended periods, a magnetisation isotherm at $T = 1.5$ K was measured up to 59 T in a pulsed magnetic field at the Dresden High Magnetic Field Laboratory. The final experimental magnetisation curve (Figure 3.9) is linear and lacks noticeable structure. Although at high fields

the curve seems to deviate from a straight line, these fluctuations often accompany a pulsed field experiment and are most likely artefacts.

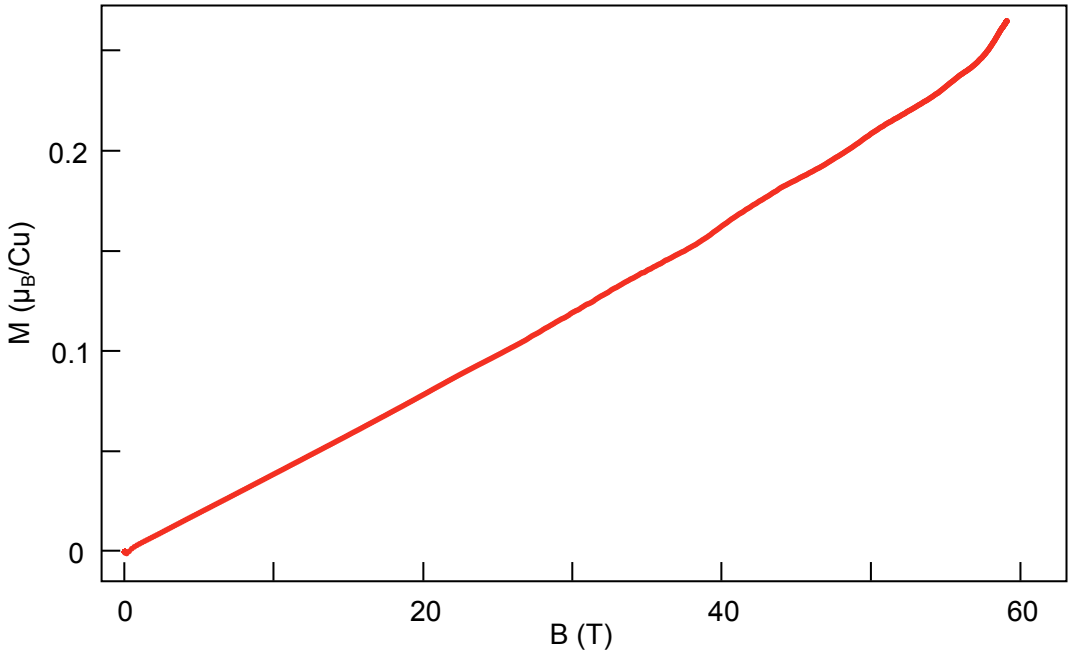

FIGURE 3.9: Experimental magnetisation isotherm at $T = 1.5$ K.

The most interesting feature of the magnetisation curve is that it starts from the origin, i.e. magnetisation starts increasing linearly already at low external fields instead of becoming non-zero only at some finite external magnetic field. This demonstrates that there either is no spin gap in Cu(OH)Cl or it is so low that lies below our experimental sensitivity. This is an indication that Cu(OH)Cl is not in the dimer phase part of the Shastry-Sutherland model quantum phase diagram. However, it is still possible that the spin gap is very small and remains undetected. This could be the case if Cu(OH)Cl were situated still in the dimer phase part of the phase diagram, but very close to the phase transition to the Néel region.

3.3.3 Heat capacity

Specific heat measurements can be useful in determining magnetic properties of materials, but it has to be kept in mind that the overall heat capacity of a sample that is measured experimentally is a superposition of contributions from various

physical effects. At moderate to high temperatures, the contribution from lattice vibrations (phonons) dominates over all the other components. According to the Debye model [53], at $T \ll T_D$ the phonon contribution is proportional to T^3, i.e. decreases very rapidly when temperature is lowered. Therefore the only region where it is possible to observe the magnetic heat capacity is at very low temperatures.

The heat capacity of Cu(OH)Cl was measured in the temperature range 2 – 30 K, first without any magnetic field and then in an applied field of 7 T (see Figure 3.10). Measurements were performed at constant pressure with the Quantum Design PPMS (Physical Property Measurement System) calorimeter. This instrument uses a thermal relaxation method for measuring heat capacities, the underlying operating principle of which is the following. The sample is first stabilised at some temperature, then a short pulse of heat is given that warms the sample up to a slightly higher temperature. The heat capacity of the sample is determined from the following exponential decay of temperature.

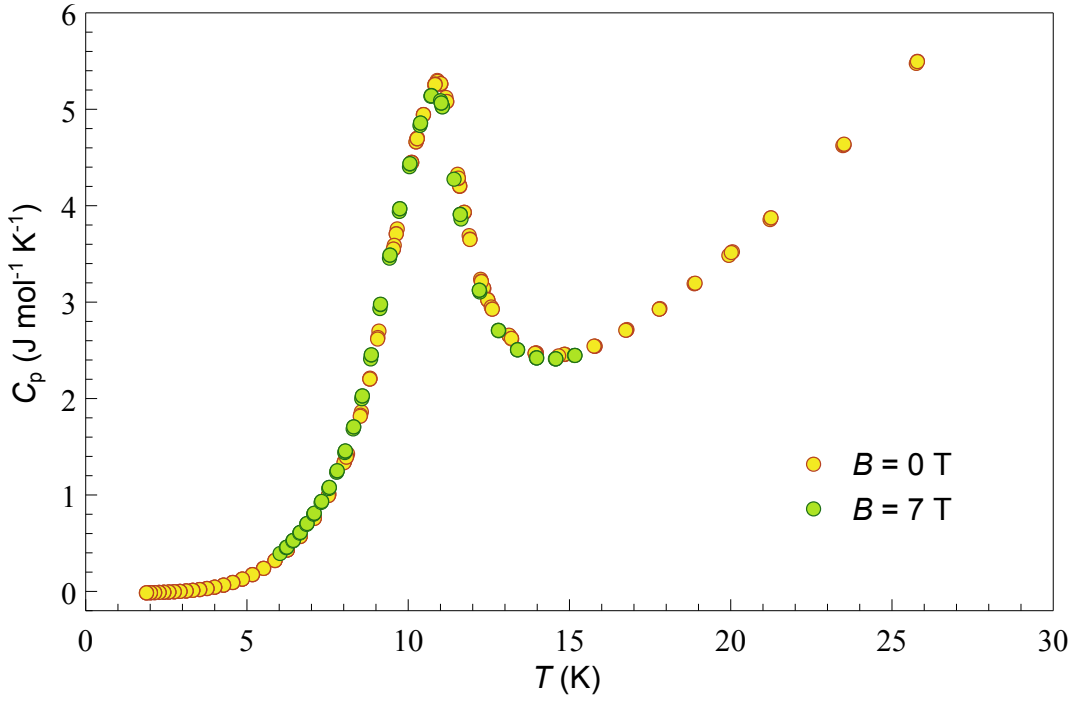

FIGURE 3.10: Specific heat, measured at $B = 0$ T and $B = 7$ T. The peak at 11 K indicates a phase transition into a magnetically ordered state.

There is a peak in specific heat with maximum at 11 K in case of both $B = 0$ T and $B = 7$ T. The peak is fairly localised and resembles a lambda-type anomaly expected for a second order phase transition. This is a very clear signature of magnetic ordering, indicating that in Cu(OH)Cl a phase transition to a state with long-range magnetic ordering occurs at 11 K. That observation is in excellent agreement with the abrupt change in slope of the magnetic susceptibility curve and the presence of a peak in the function $d(\chi T)/dT$, all at 11 K.

Based on the analysis of experimentally measured susceptibility, magnetisation and specific heat curves, it can thus be concluded with high certainty that if Cu(OH)Cl follows the Shastry-Sutherland model, then it has to lie in the Néel phase part of the phase diagram.

4. Methods

4.1 *Ab-initio* calculations

4.1.1 Principles of density functional theory

Ab-initio calculations carried out in this work were based on DFT, a powerful method that allows calculating the ground state electron density (and related properties) of a system when only given the crystal structure. The main ideas behind DFT are summarised by the Hohenberg-Kohn theorem [54]. It states that the ground-state electron density of a system defined by an external potential uniquely determines the Hamiltonian operator, so that when the former is known, all other properties of the system can be calculated in principle, including the many-body wave function. Furthermore, this ground state electron density can be obtained by variational methods, more precisely by minimising the ground state energy functional.

The main reason for the appeal of DFT is that the ground state electron density can be calculated without having to know the ground state wavefunction. All that is needed is an expression of the ground state energy as a functional of the electron density. The problem here is that the explicit form of this expression is not known.

In the Kohn-Sham framework [55], the ground state electron density is expressed in terms of a fictitious system of non-interacting electron orbitals with the same ground state density as the original system of electrons. Now the problem can

be reduced to a collection of standard single-particle differential equations, with the particles moving in an effective potential that depends on the overall electron density. After solving this set of equations self-consistently in a series of iterations, the ground state electron density can be extracted.

The final remaining problem with Kohn-Sham equations is that in addition to simple Coulomb interaction parts, the effective potential contains a term for which an exact expression is not available generally, namely the exchange-correlation functional. Several schemes of approximating the exchange-correlation functional have been proposed, for each of which many different parametrisations exist. Calculations carried out in this work were based on two schemes: the local density approximation (LDA) and the generalised gradient approximation (GGA).

Homogeneous free electron gas is the only system for which the exact expression of the exchange-correlation functional is known. In LDA, each small volume of electrons is treated locally like a uniform free electron gas, the full exchange-correlation functional is obtained simply by integrating over the whole system [56]. This very basic approach works surprisingly well, which has made LDA the most widely used approximation. LDA can be easily generalised to take into account electron spin, thus leading to local spin density approximation (LSDA) [57].

There are some well-known problems with LDA, for example it systematically underestimates the band gap [58]. While this particular issue is not a big concern in this work, where the band gap depends on strong Coulomb correlations anyway, sometimes more precise results can be obtained with generalised gradient approximation. GGA is also a local approximation scheme, but in addition to the value of electron density in each small volume, the gradient of electron density is taken into account as well [59]. For some of our purposes, results of LDA and GGA are known not to differ significantly [29] – in these cases, LDA was preferred due to its robustness. However, in DFT+U calculations (Section 4.1.2) even tiny differences in ground state energy can have a big impact on predicted values of exchange couplings. To ensure better precision of DFT+U results, GGA (in Perdew–Burke–Ernzerhof 1996 parametrisation [60]) was invoked.

4.1.2 DFT calculations on Cu(OH)Cl

In this work, all DFT calculations were carried out using the full-potential scalar-relativistic code FPLO9.05-39 [61]. In FPLO, the solution to Kohn-Sham equations is constructed as a linear combination of overlapping local orbitals, which means that the crystal potential consists of localised overlapping potential contributions. As opposed to many other codes where the basis set for a periodic system is made out of plane waves (or similar) for computational convenience, the basis set of atomic-like orbitals in FPLO carries chemical information. This allows to project the final electron density on local orbitals straightforwardly, making extraction of model parameters from band structure calculations more reliable. In comparison with other tools, the main strength of FPLO is that the crystal potential is fully taken into account, as opposed to using pseudopotentials for approximating it. Also, core electrons are treated in the same way as valence electrons. All this increases the accuracy of results computed by FPLO, but of course brings with it the inevitable trade-off in computation times, limiting the size of systems that can be investigated.

All initial calculations (relaxing the hydrogen position and evaluating the band structure) were done using LDA with Perdew-Wang parametrisation [62] for the exchange-correlation potential. The process of finding the relaxed location of the hydrogen atom was performed by carrying out a cycle of LDA calculations. Each step of the cycle included calculating the electron density for the structure, finding the force on the hydrogen atom and adjusting its position. This was repeated until the force on the H atom was below 10^{-2} eV/Å.

The first estimate of the microscopic magnetic model of Cu(OH)Cl was obtained from its LDA band structure. This is not straightforward – LDA calculations are not spin-polarised and correlation effects in the Cu 3d shell are not taken into account. However, an indirect approach exists that allows us to utilize the LDA band structure. As predicted by crystal field theory (Section 5.1.1), the highest occupied bands in Cu(OH)Cl arise from Cu $3d_{x^2-y^2}$ atomic orbitals. Therefore if

we use the tight-binding approximation on these orbitals, we can obtain hopping parameters between them by fitting the relevant bands. Finally, these hopping parameters between half-filled orbitals can be analysed with the Hubbard model (Section 2.1), which gives us the values of antiferromagnetic exchange couplings between Cu sites.

Instead of fitting the LDA band structure manually, the procedure of obtaining a tight-binding fit can be automatised with the help of Wannier functions [63]. In our case, a Wannier function was constructed from the $3d_{x^2-y^2}$ atomic orbital of each Cu site in the unit cell. Running the fitting procedure on the band structure then resulted in the set of best-fitting hopping parameters between Wannier functions centred at different Cu atoms. The tight-binding model was mapped on a one-orbital Hubbard model with effective on-site Coulomb repulsion $U_{\text{eff}} = 4.5$ eV, the value found to be appropriate for Cu^{2+} $3d$ orbitals in cuprates [49, 64, 65].

In the strongly correlated regime $t \ll U_{\text{eff}}$, a good approximation for the antiferromagnetic contribution to a coupling originating from superexchange can be found using second-order perturbation theory: $J_{\text{AFM}} = 4t^2/U_{\text{eff}}$ [12]. Even though the results obtained by using this formula neglect the ferromagnetic contribution, they still give us the first estimate about which couplings are important for the microscopic magnetic model. Furthermore, as we expect superexchange to be the dominant pathway giving rise to couplings between Cu sites, results obtained in this manner should correspond reasonably well to reality.

To get another estimate of numerical values of exchange couplings, we carried out DFT+U calculations. This is an alternative way for taking into account correlation effects in the Cu 3d shell, and it should incorporate both ferro- and antiferromagnetic contributions to J-values [66]. DFT+U calculations are spin-polarised, meaning that calculations can be started from various initial spin configurations and result in a different ground state energy for each configuration. Additionally, correlation effects for specified orbitals are included by assigning an energy penalty U_d for double occupancy of these orbitals.

For Cu(OH)Cl, total energies of various collinear spin configurations were calculated using this method and mapped onto the classical Heisenberg model. To be able to assign different initial magnetic moments to different Cu sites, symmetry of the unit cell was reduced to P1. Additionally, the size of the unit cell was doubled in the crystallographic a-direction. This way we were able to look into both intra- and interlayer couplings. By subtracting total energies of suitably chosen initial spin configurations from one another, values for exchange couplings between Cu sites were obtained.

We used the fully localised limit double counting scheme with the on-site Coulomb repulsion parameter in the range $U_d = 8.5 \pm 1.0$ eV and the Hund's exchange parameter $J_d = 1$ eV. This choice of parameters follows previous studies, best results have been obtained by using those U_d values [50]. The final U_d was chosen in such a way that it would reproduce the θ-temperature $\theta = 80$ K determined from experimental data in section 3.3.1. As an additional measure, we verified that varying the U_d value by up to 0.5 eV did not make a qualitative difference to our results.

In all DFT calculations, k mesh density was increased until convergence of results was achieved. For LDA calculations (4 symmetry-inequivalent atoms), this meant using 1728 k points in the symmetry-irreducible part of the Brillouin zone, whereas for DFT+U calculations (32 symmetry-inequivalent atoms), 64 k points were enough to achieve convergence.

4.2 Model simulations

After a microscopic magnetic model has been constructed for a compound, it is the next logical step to predict the physical properties that arise from that model and compare these with experiment. Of the experimental data available for Cu(OH)Cl, magnetic susceptibility and magnetisation curves are of most interest for that purpose. The heat capacity data includes a phonon contribution and thus cannot be directly fitted.

There are several methods that enable simulations of thermodynamic properties of microscopic magnetic models. In this work, two complementary approaches were taken: diagonalisation of the Hamiltonian and high temperature series expansions. The usual method of choice for these tasks is Quantum Monte Carlo, but it was not used in this work. Quantum Monte Carlo simulations allow direct modelling of the many-body wavefunction and thus often give very good results, but this tool cannot be used to analyse strongly frustrated systems and was therefore not applicable to Cu(OH)Cl [67].

4.2.1 Diagonalisation of the Hamiltonian

The Hamiltonian operator of a spin system can be represented as a matrix, the eigenvalues of which can be found by diagonalising it. Once the energy eigenvalues have been obtained, one can proceed and calculate other thermodynamic quantities from it, including magnetic susceptibility, magnetisation isotherms and magnetic heat capacity. This method is in principle completely accurate as it does not involve any computational approximations, and should therefore give reliable predictions for physical properties of the system [68].

The problem with diagonalisation is that the Hilbert space of a collection of N spin-$\frac{1}{2}$ particles has the dimension 2^N. It means that the size of the Hamiltonian matrix grows exponentially with the number of particles, and so do computation times. This places a very sharp limitation on the maximum size of a system that can be investigated using diagonalisation methods in reasonable time. Periodic boundary conditions can be used to extend size of the system seemingly up to infinity, but this still fails to capture phenomena that occur at larger scales than a unit cell (or are incommensurate with it). Especially in case of strongly frustrated models, the behaviour of a small system can be very different from a macroscopic one. Therefore diagonalisation results have to be treated with caution for finite size effects, especially when calculated for low temperatures [68].

In addition to exact diagonalisation (ED) where all eigenvalues of a matrix are precisely calculated, there are methods that utilise the sparsity of Hamiltonian matrices, most notably the Lanczos algorithm [69]. Also, for some applications only the lowest-lying eigenvalues are of importance. When these simplifications are taken into account, slightly larger systems can be treated than by basic exact diagonalisation. Still, currently systems with more than several tens of sites are out of reach of diagonalisation methods.

In this work, exact diagonalisation simulations were carried out using the ALPS simulation package (http://alps.comp-phys.org/) [70]. A square lattice consisting of a single layer of 16 spin-$\frac{1}{2}$ sites with periodic boundary conditions was constructed, interactions between sites arranged according to the Shastry-Sutherland model. Many different sets of values for exchange couplings were investigated, for each of which magnetic susceptibility and magnetisation curves were calculated. In addition, O. Janson performed Lanczos diagonalisation on our final model to calculate the magnetisation curve more precisely on a lattice of 24 atoms.

As discussed in Section 2.2, two-dimensional models cannot undergo long-range magnetic ordering and thus we cannot expect to see any signs of that in diagonalisation results. Also, finite size effects have to be kept in mind when analysing the low-temperature regions of simulated curves, especially due to strong frustration present in Cu(OH)Cl.

4.2.2 High temperature series expansions

Series expansions present another way for predicting thermodynamic properties of a microscopic magnetic model. This method has its roots in statistical physics, the starting point of it being the partition function of the system. In principle, thermodynamic quantities like magnetic susceptibility and heat capacity can be obtained from the partition function via appropriate manipulations, but again due to the macroscopic size of any real system it is impossible in practice. However, the expressions for thermodynamic properties can be expanded as power series of

$\beta = 1/k_B T$, and it is possible to estimate numerically the values of coefficients for terms with lowest powers of β. At high enough temperatures higher-order terms become negligible and the series give reasonable estimates of thermodynamic properties [71].

Based on the microscopic magnetic model constructed using DFT results, J. Oitmaa calculated several high temperature series expansions (HTSE) of magnetic susceptibility. For various sets of model parameters, series coefficients were obtained for terms up to 10^{th} order in β (see Appendix A for the values of the coefficients). Symmetric Padé approximation was performed on the series to increase their temperature region of validity [72]. Using these Padé approximants, we managed to get good fits of the experimental magnetic susceptibility curve down to 100 K. Estimates for values of exchange couplings were extracted from the fitted parameters. Finally, the fits were compared with one another according to their sum of squared residuals to determine the one with best quality.

HTSEs do not output the physical magnetic susceptibility function, but rather a reduced susceptibility curve. To fit experimental data with a HTSE, it has to be scaled using g, J and values of some physical constants (see Appendix A for details). That way in addition to J, the value of g can also be extracted from the fit and then compared with the range of expected g-values for Cu^{2+} compounds. Moreover, we included an extra temperature-independent fitting parameter $+\chi_0$ to correct for the diamagnetism of filled electron shells (core diamagnetism) [73]. The fact that the fitted value of this parameter was always very small and negative shows that χ_0 really corresponded to core diamagnetism, thus justifying its inclusion.

5. Results

5.1 *Ab-initio* calculations

5.1.1 LDA density of states and band structure

The first set of *ab-initio* results were obtained from LDA calculations. Even though the principal result of these calculations is the ground state electron density, that quantity itself is not very helpful for understanding the physics of the system. Instead, it is informative to visualise the density of states (DOS) and the band structure (Figures 5.1 and 5.2, respectively).

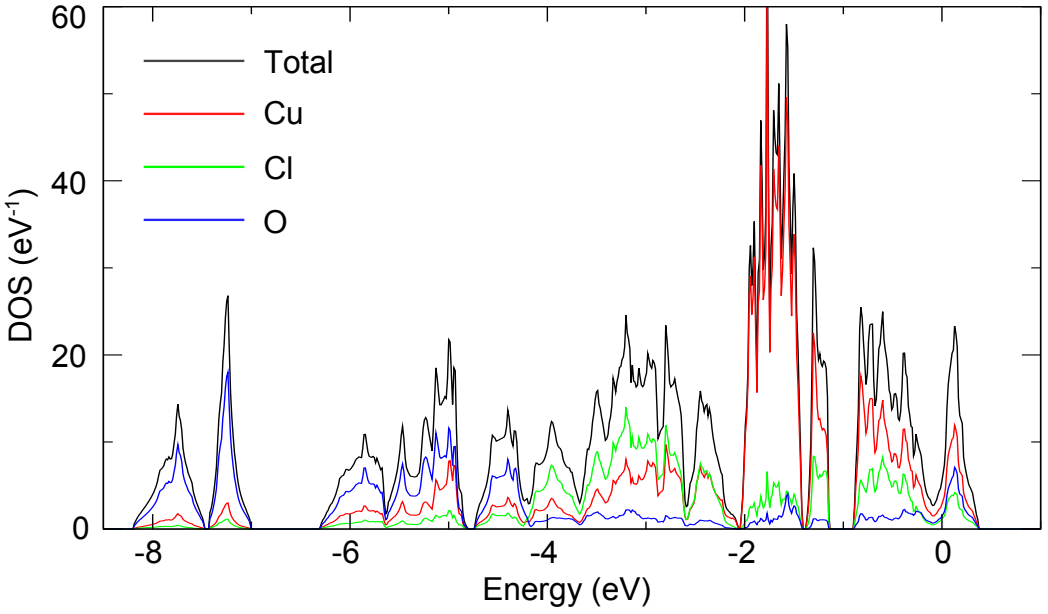

FIGURE 5.1: LDA density of states. The Fermi level is at zero energy, non-zero DOS there is an artefact of using LDA. The isolated group of states near the Fermi energy originates from Cu^{2+} e_g orbitals.

At first glance, the density of states and the band structure seem inappropriate for an insulator like Cu(OH)Cl – the DOS at the Fermi level is non-zero, indicating that the compound is metallic. This is a shortcoming that accompanies our use of an approximation like LDA. In reality, the correlations effects in Cu^{2+} partially filled 3d orbitals play a significant role, but they are not taken into account in LDA. However, we can regard the LDA band structure as a first approximation and treat correlations either on the model level or by the use of DFT+U.

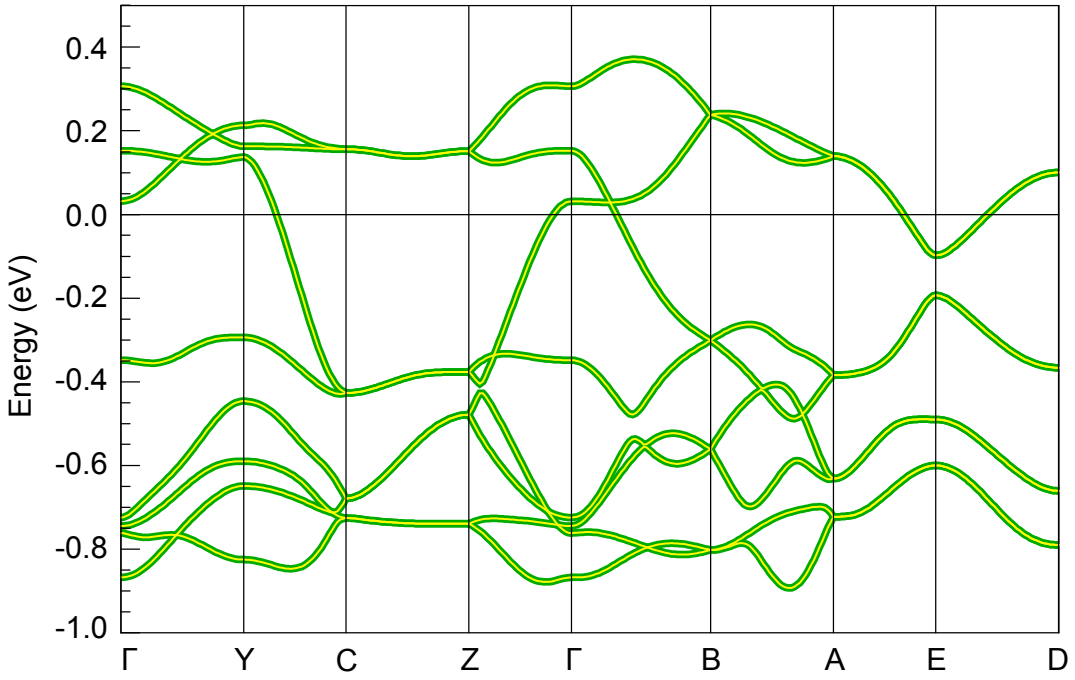

FIGURE 5.2: LDA band structure (yellow lines) showing the Cu^{2+} $3d_{x^2-y^2}$ and $3d_{3z^2-r^2}$ bands near the Fermi energy, together with its Wannier function fit (green lines). The k path is defined as $\Gamma(0,0,0)$, $Y(0.5,0,0)$, $C(0.5,0.5,0)$, $Z(0,0.5,0)$, $\Gamma(0,0,0)$, $B(0,0,0.5)$, $A(0.5,0,0.5)$, $E(0.5,0.5,0.5)$, $D(0,0.5,0.5)$.

With the help of crystal field theory, we can rationalise the qualitative features in the DOS and the band structure despite the shortcomings of LDA. Due to the octahedral environment experienced by Cu atoms, we expect the Cu $3d_{x^2-y^2}$ and $3d_{3z^2-r^2}$ (i.e. the e_g orbitals) to be the two highest occupied orbitals. Here, x, y and z denote the local crystallographic axes: x and y point from the Cu site towards ligands and z is perpendicular to them. The three t_{2g} orbitals should lie lower in energy [74].

This is consistent with what we observe in LDA results. In the DOS, there is a narrow isolated region of bands around the Fermi level (from e_g orbitals) – from

the band structure we can count that it consists of 8 bands (2 bands per Cu atom) as expected. Because the environment of a Cu^{2+} ion is elongated in the z-direction, crystal field theory allows us to assign Cu^{2+} $d_{x^2-y^2}$ orbital character to the upper 4 bands. Since these are the bands that contain the unpaired electrons, they are the most relevant for the purposes of understanding magnetism in Cu(OH)Cl. The next set of 4 bands, based on Cu^{2+} $d_{3z^2-r^2}$ orbitals, occupy a nearly separate energy window than the $d_{x^2-y^2}$ bands. From all that we conclude that the unpaired electron on each Cu site should be in an orbital resembling $3d_{x^2-y^2}$.

The next collection of bands lie at much lower energies, between -2 and -1.2 eV, and correspond to the three Cu t_{2g} orbitals. Going even further, we find the oxygen $2p$ and chlorine $3p$ states. All these bands have little to do with the magnetic properties displayed by Cu(OH)Cl.

5.1.2 Wannier function fit of LDA band structure

The LDA band structure plot in Figure 5.2 consists of two almost non-overlapping groups of 4 bands. As discussed before, the higher group originates from the Cu $3d_{x^2-y^2}$ orbitals, with x- and y-axes pointing towards neighbouring O and Cl atoms, and contains one band for each Cu atom in the unit cell. As our first attempt to take correlation effects into account, we mapped the band structure on a tight-binding model by fitting the band structure with Wannier functions. Even though the Cu^{2+} $d_{x^2-y^2}$ were situated in a nearly separate energy window, we fitted the whole set of 8 bands for better precision. This meant using two Wannier functions per Cu atom, one based on the $3d_{x^2-y^2}$ (visualised in Figure 5.3) and the other on the $3d_{3z^2-r^2}$ orbital.

The fitting process resulted in hopping parameters between Wannier functions, including those that correspond to a pair of orbitals on different Cu sites. To proceed and obtain estimates for exchange couplings, the tight-binding results need to be mapped on a Hubbard model. In that framework, however, only a single orbital per site should be taken into consideration, therefore only the hopping

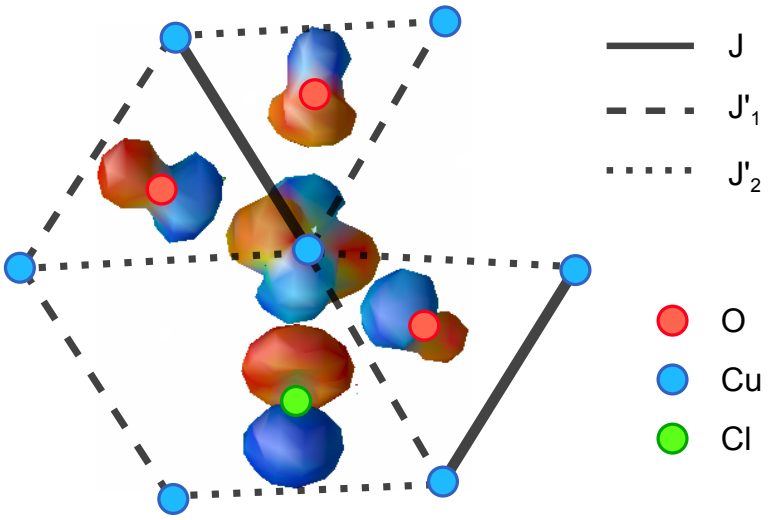

FIGURE 5.3: Visualisation of the Wannier function based on the Cu^{2+} $d_{x^2-y^2}$ orbital. The nearest Cu sites are included as well, together with the strongest interlayer exchange couplings obtained by fitting the band structure.

parameters between $3d_{x^2-y^2}$-based Wannier functions were used to calculate the couplings. This simplification was justified since the fitted values for hoppings between Wannier functions with differing orbital characters were small – a consequence of $3d_{x^2-y^2}$ and $3d_{3z^2-r^2}$ bands lying at different energies.

The main hopping parameters and exchange coupling values obtained by this method are listed in Table 5.1, together with relevant distances and angles between Cu sites. Three of the important couplings lie within the layers of Cu(OH)Cl (J, J_1', J_2') and one is between atoms from different layers (J_{int}). We neglected the rest of the in-plane couplings as they were at least an order of magnitude smaller than the in-plane ones listed in Table 5.1 and thus do not have a significant impact on the magnetic properties of Cu(OH)Cl. For the same reason, only the largest interlayer coupling (J_{int}) was included in the model.

5.1.3 DFT+U results

The method of fitting LDA band structure is good for determining which exchange couplings are large enough to matter for the microscopic magnetic model. However, since only the antiferromagnetic contributions to couplings were estimated this way, true values are usually lower due to ferromagnetic interactions.

TABLE 5.1: The list of main *ab-initio* exchange couplings from LDA band structure fit and DFT+U calculations. Each coupling is characterised by the distance between Cu sites and the Cu-O-Cu angle between the bonds along which the Cu sites are connected. The couplings are visualised on the crystal structure in Figures 5.4 and 5.5.

	Cu-Cu distance (Å)	Cu-O-Cu angle	LDA t (meV)	LDA J_{AFM} (K)	GGA+U J (K)
J	3.03	98.8°	168	291	52
J_1'	3.29	109.5°	119	146	59
J_2'	3.36	114.0°	122	154	64
J_{int}	8.06		68	48	21

This means that the results so far only indicate the order of magnitude of various couplings. To obtain better quantitative estimates, we carried out GGA+U calculations.

As explained in Section 4.1.2, a precise value that should be used for the on-site Coulomb repulsion parameter U_d is never known *a priori*. For a new compound, a range of U_d values has to be tested, and exchange couplings calculated each time. In case of Cu(OH)Cl, the GGA+U results obtained by varying U_d were all qualitatively reasonable and in agreement with one another. The final value, $U_d = 9.5$ eV was selected because it reproduced the θ-temperature $\theta = 80$ K determined from experimental data in section 3.3.1.

The final estimates of GGA+U couplings with $U_d = 9.5$ eV are listed in Table 5.1. When we compare these values with the ones obtained by fitting the LDA band structure, we see that they differ by ~ 250 K or ~ 100 K for J and J', respectively. This difference comes from ferromagnetic contributions to exchange couplings that were taken into account in DFT+U but had been neglected by LDA.

5.1.4 *Ab-initio* microscopic magnetic model for Cu(OH)Cl

From LDA band structure fitting and DFT+U calculations, we have ascertained that there are three important exchange couplings of similar magnitude within a Cu(OH)Cl layer, plus a three times weaker coupling between the layers. The system is therefore quasi-two-dimensional, but the interlayer coupling is not weak enough to be completely neglected. These four couplings constitute our first microscopic magnetic model of Cu(OHC)Cl and are visualised on the crystal structure in Figures 5.4 and 5.5.

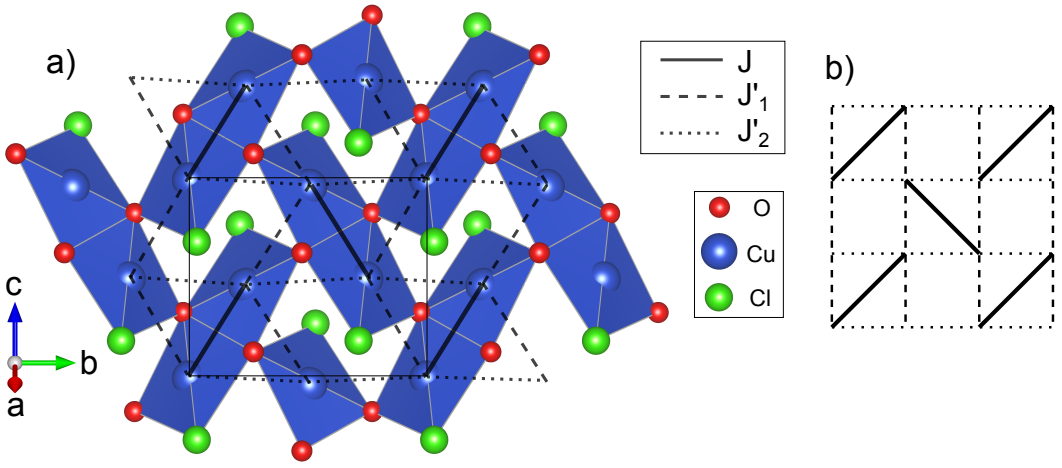

FIGURE 5.4: a) Significant exchange couplings within a layer of Cu(OH)Cl, as determined by LDA and DFT+U calculations. b) For comparison, the corresponding fragment of the Shastry-Sutherland lattice.

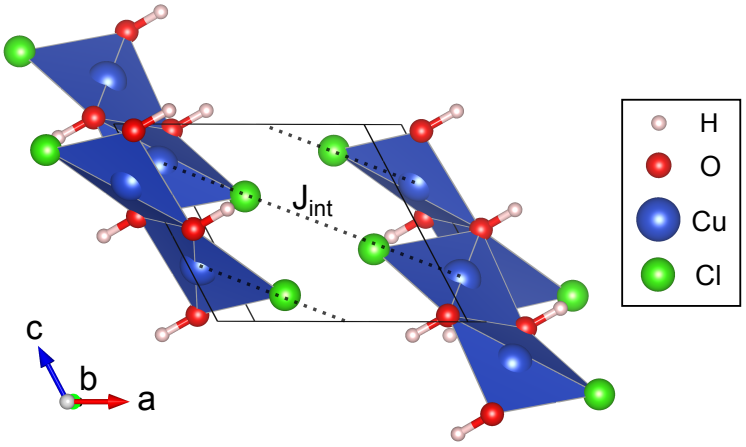

FIGURE 5.5: The interlayer exchange coupling J_{int}.

As can be seen in Figure 5.4, the exchange couplings within a layer form a Shastry-Sutherland lattice, confirming the expectation based on the crystal structure. The

antiferromagnetic intradimer coupling (J) is frustrated by the two antiferromagnetic interdimer couplings (J_1' and J_2') that pass through the neighbouring Cu site and have the opposite effect on the magnetic moments of the dimer. Properties of the spin-1/2 antiferromagnetic Shastry-Sutherland lattice have been thoroughly studied (see Section 3.2). However, most studies have focused on models where couplings J_1' and J_2' are equal, but from *ab-initio* results it is clear that this is not necessarily the case in Cu(OH)Cl.

Additionally, we have a sizeable interlayer coupling, which could create a noticeable difference between the magnetic properties of Cu(OH)Cl and simple Shastry-Sutherland lattice-based model systems. When the precise arrangement of interlayer couplings is investigated, it turns out that they are not frustrated and thus should simply assist magnetic ordering (as was explained in Section 2.2) instead of giving rise to other, more complicated effects. Another argument that diminishes the importance of interlayer couplings is that there is only a single J_{int} per Cu site. In most models, interlayer couplings link each magnetic site with two others, one in the previous and one in the following layer, so we can say that the effective interlayer coupling in our model is only half of J_{int}.

Despite the aforementioned shortcomings, the basic Shastry-Sutherland model bears many similarities with our *ab-initio* results and thus forms a good starting point for further analysis.

5.2 Model simulations

Having constructed a microscopic magnetic model, we would like to simulate the thermodynamic properties of Cu(OH)Cl based on that. Fitting the simulation results to experimental data would then allow us to determine model parameters (exchange couplings) with higher accuracy. The problem with the values of couplings obtained from *ab-initio* calculations is that there is a great deal of approximation involved and they might not correspond to reality precisely – fitting experimental results with our model allows us to do better.

Which thermodynamic properties can be used for fitting? In Section 3.3, experimental curves of magnetic susceptibility, specific heat and magnetisation were described. A limited amount of information was extracted from the magnetisation isotherm, but fitting a nearly featureless straight line would not give us the values of four exchange couplings. Specific heat data cannot be used either, because it is a superposition of contributions from several different mechanisms. The information about exchange couplings is carried in the *magnetic* heat capacity curve, which is completely overpowered by the phonon contribution at temperatures higher than 10-20 K. On the other hand, we are hindered from using the low-temperature part by the fact that simulation techniques tend to break down at temperatures that go much below the magnitudes of exchange couplings. All this leaves only the magnetic susceptibility curve as suitable for fitting – it has got interesting features and can be simulated reasonably well within the temperature range of our experimental results.

The biggest drawback of this whole approach is that only a small number of parameters can be reliably determined from fitting the experiment. There are four independent exchange couplings in the *ab-inito* model for Cu(OH)Cl – this is too much and would lead to overfitting, especially since only the magnetic susceptibility curve can be used. Therefore before we can fit the experimental data and extract values for exchange couplings, our model needs to be simplified. Two sets of simulations were carried out to assess the suitability of simplifications: exact diagonalisation of the model Hamiltonian and high temperature series expansions of magnetic susceptibility.

5.2.1 The difference between J_1' and J_2'

The first plausible alteration towards getting a simpler microscopic magnetic model is taking $J_1' = J_2'$. Not only would it decrease the number of fitting parameters, but it would allow us to access the wealth of previous theoretical results about the conventional Shastry-Sutherland model. According to our *ab-initio* results (Table 5.1), this would be quite a small approximation: the difference between the

values estimated for J_1' and J_2' was under 10%. Nevertheless, it is conceivable that even this small difference can have a noticeable effect to physical properties of the system – especially due to the delicate nature of phenomena that arise from strong geometrical frustration. To establish whether this is the case or not, we investigated the effects of this approximation with the method of exact diagonalisation.

When the Heisenberg model Hamiltonian corresponding to a lattice of exchange couplings is diagonalised, its energy spectrum is obtained. The thermodynamic properties of the model then follow straightforwardly. By varying the values of J_1' and J_2' and applying this method to each model, one can investigate the effect that exchange couplings have on the magnetic susceptibility curve. Initially, we imposed the restriction $J_1' = J_2' = J'$ and varied the average interdimer coupling J' to see its effect on magnetic susceptibility (Figure 5.6). Alternatively, we fixed the average of $J_1' = J_2'$ at $J' = 0.75J$ and varied J_1' and J_2' (Figure 5.7).

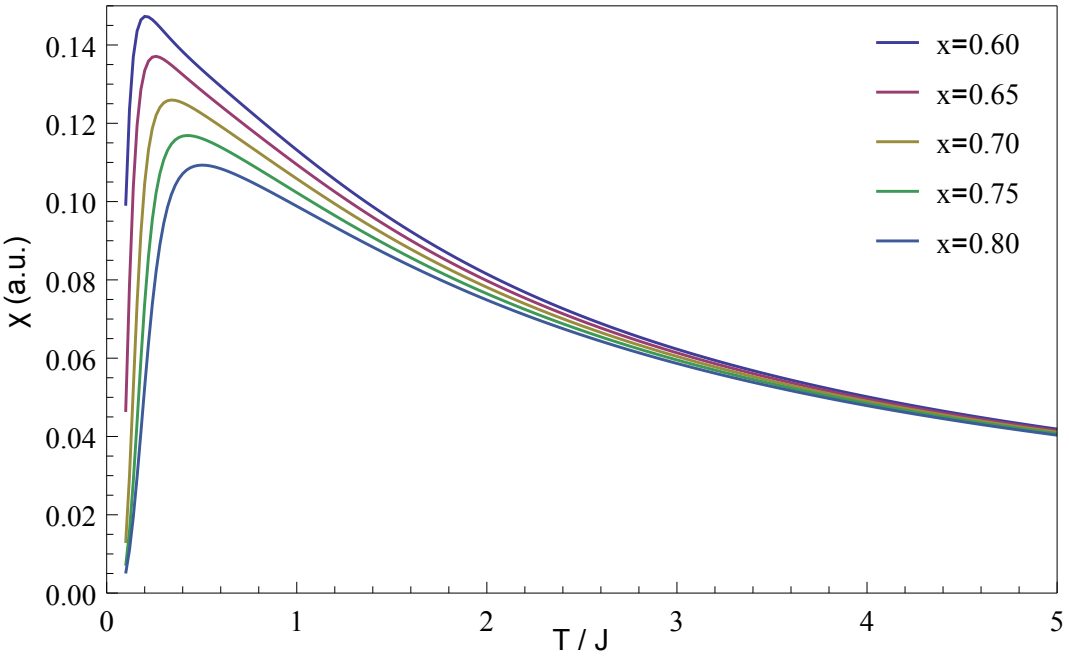

FIGURE 5.6: Exact diagonalisation simulations of magnetic susceptibility: the effect of varying the average $J' = J_1' = J_2'$, reported via $x = J'/J$.

As can be seen from the results, the effect of having a 14% difference between J_1' and J_2' is negligible, whereas changing the average interdimer coupling by the same fraction makes a pronounced difference to the magnitude and position of the susceptibility maximum. It is also clear that in both cases, the effect on the

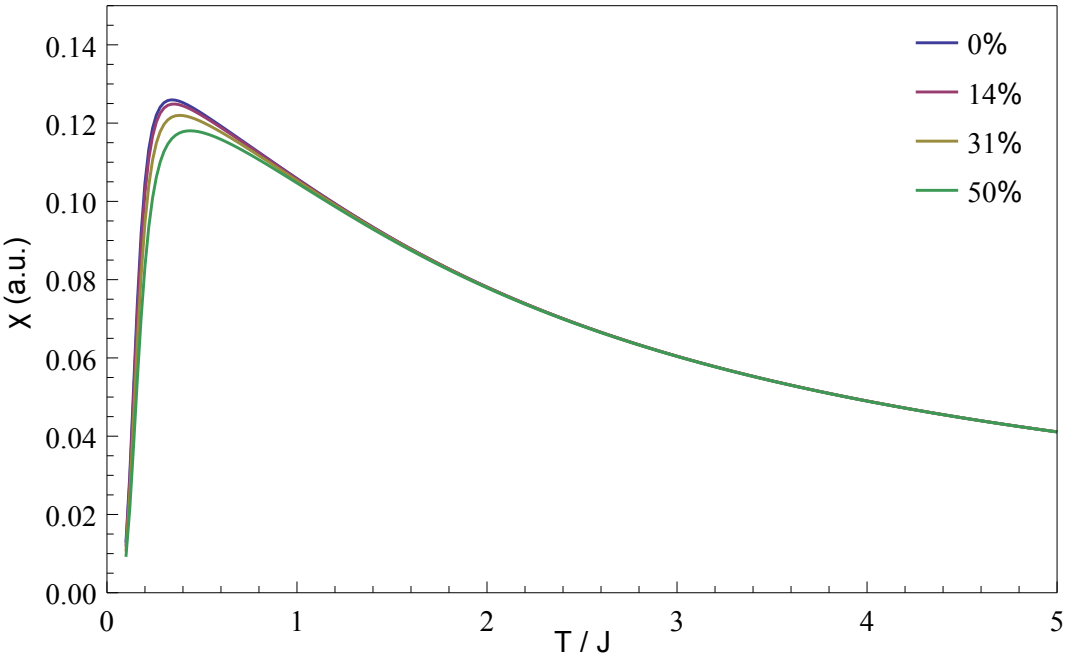

FIGURE 5.7: Exact diagonalisation simulations of magnetic susceptibility: the effect of having different J_1' and J_2'. The relative difference $(J_1' - J_2')/J_1'$ was varied while keeping the average constant, $(J_1' + J_2')/2J = 0.75$.

magnetic susceptibility decreases upon moving to higher temperatures. However, the curves converge much more rapidly in the case when $J_1' \neq J_2'$ than when we vary a single J' value. This is very important for our purposes, because we will be fitting mostly the high-temperature region of the experimental magnetic susceptibility curve. Therefore according to the results of exact diagonalisation, the average of J_1' and J_2' plays a much greater role in the magnetic susceptibility curve than their difference – we can safely ignore the fact that there are two different interdimer couplings and use just a single J'.

5.2.2 The effect of interlayer couplings

Even after making the approximation that $J_1' = J_2'$, there are still three independent parameters left in our microscopic magnetic model: the intradimer coupling J, the interdimer coupling J' and the interlayer coupling J_{int}. The first two of these are inherent to the Shastry-Sutherland model and thus also form a key part of our microscopic model. However, because the interlayer couplings are not frustrated and only link each site with one neighbouring layer (see Section 5.1.4), one might

hope that the magnetic susceptibility curve depends only weakly on the value of J_{int}. On the one hand, this would mean that it is difficult to reliably determine the strength of the interlayer coupling, but on the other hand it might allow us to refrain from including J_{int} as an independent fitting parameter.

Based on *ab-initio* simulation results, we expect J_{int} to be roughly by a factor of two weaker than J'. Therefore as a first approximation, we can take $J_{\text{int}} = 0.5J'$ and then investigate how much the precise value of J_{int} affects the susceptibility curve and the fitted values of exchange couplings. For that purpose, high temperature series expansions of magnetic susceptibility were calculated for various values of J_{int}. To simplify the process of finding the HTSEs, all couplings within a layer were taken to be equal, $J = J'$.

The obtained dependence of the fitted value of J' from the ratio J_{int}/J' (Table 5.2) was very weak, under $\pm 2\%$ for reasonable values of J_{int}/J'. These results prove that the effect of the interlayer coupling on the susceptibility curve is small and justify fixing the ratio J_{int}/J' to its DFT estimate $J_{\text{int}} = 0.5J'$. Even if the true value of J_{int} is slightly different, our approximation should remain reasonable since the physics of the system is dominated by the strongly frustrated couplings within layers of Cu(OH)Cl.

TABLE 5.2: Dependence of the fitted value of $J = J'$ on the ratio J_{int}/J'. Since the interlayer coupling influences the fitted J' very weakly, we can set its value at $J_{\text{int}} = 0.50J'$.

J_{int}/J'	Fitted J' (K)
0.40	60.9
0.45	60.6
0.50	60.2
0.55	59.8
0.60	59.4

5.3 Microscopic magnetic model for Cu(OH)Cl

After making simplifications and establishing the validity of our approximations, it is possible to fit the experimental magnetic susceptibility data and obtain estimates of model parameters. This is best done using the HTSE curves, because they include the effect of interlayer couplings. In addition to that, it is informative to compare the susceptibility and magnetisation data with ED curves to verify the fitting results.

To finally obtain estimates for the values of J and J', HTSEs of magnetic susceptibility were calculated for various values of $J'/J = 0.60 \ldots 0.80$ with J_{int}/J' fixed to 0.5. The experimental susceptibility curve was fitted with each of these simulated functions, so that for each ratio J'/J estimates of all exchange couplings were obtained. To determine the best set of model parameters, the fits were compared with one another according to the sum of residuals squared (SRS) of data points.

There is a small problem with this approach, though. Since HTSEs are inherently designed to work at high temperatures, experimental data can only be fitted down to some temperature T_{min}. On the one hand, it is beneficial to use a very low value of T_{min} to include many data points and take into account the behaviour of the system as fully as possible. On the other hand, if the fitting range contains points for which the HTSE prediction is already inadequate, the resulting values of exchange couplings become inaccurate.

To ensure the validity of our results, we carried out the process of fitting susceptibility data with several HTSEs for many different values of T_{min}. For each T_{min}, the SRS values of J'/J fits were plotted and analysed - the $T_{\mathrm{min}} = 60$ K graph is given as an example in Figure 5.8. In all cases, we found that SRS values had a clear minimum. However, since our HTSEs were performed only at 0.05 intervals of J'/J, determining the position of the minimum with better precision than ± 0.025 required more effort than just selecting the lowest-lying point. The three data points with lowest SRS values were fitted with a parabola and the position of

the parabola's minimum was calculated from its equation – this formed the best estimate of J'/J for a given T_{min}.

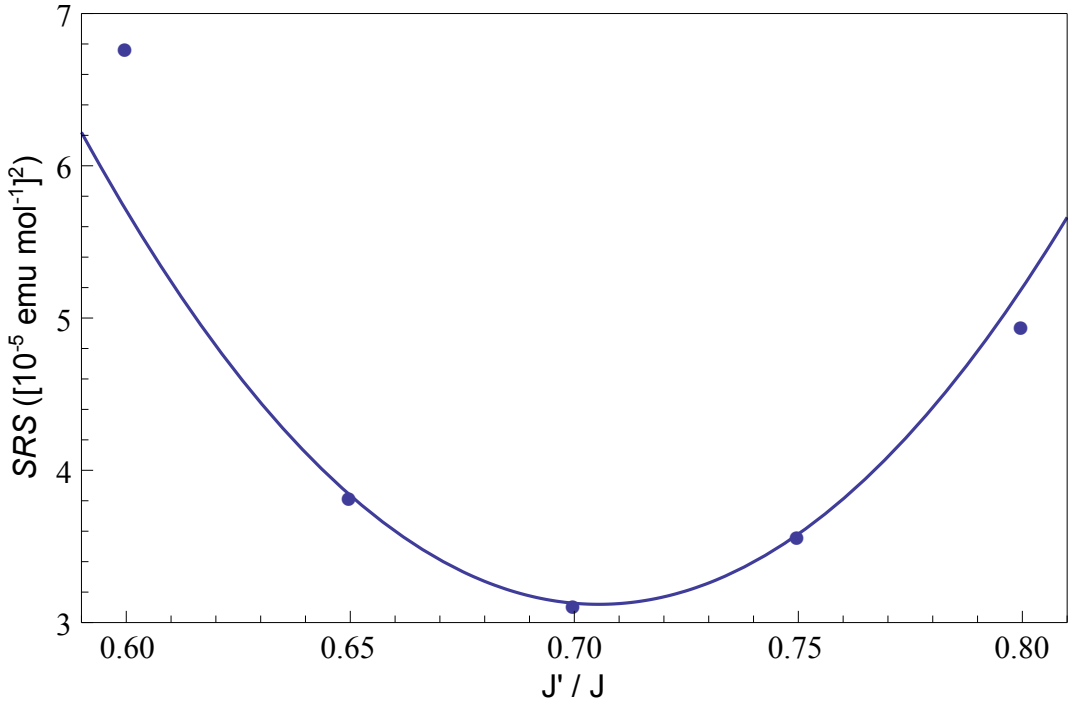

FIGURE 5.8: The sum of residuals squared (SRS) values of $T_{\text{min}} = 60$ K HTSE fits with different J'/J values. Position of the minimum was refined by fitting the three lowest-lying points with a parabola.

Best estimates of J'/J for various values of T_{min} are plotted in Figure 5.9. From this graph it is clear that the fits give consistent results down to $T_{\text{min}} = 100$K, after which the fitting range extends beyond the temperature region where HTSEs converge properly. The stable best estimate above $T_{\text{min}} = 100$ K, $J'/J = 0.75$ was extracted from the graph as our expected ratio of inter- and intradimer couplings.

The final values for exchange couplings were determined by fitting the experimental magnetic susceptibility data with the $J'/J = 0.75$ HTSE. The results were fairly robust, consistently giving $J = 80$K above $T_{\text{min}} = 80$K. According to the relations between J, J' and J_{int}, this leads to the final exchange coupling values $J = 80$K, $J' = 60$K and $J_{\text{int}} = 30$K and thus concludes the search for the microscopic magnetic model for Cu(OH)Cl.

A similar fitting process was carried out with susceptibility curves obtained from ED simulations. The only difference from the procedure described for HTSE fitting

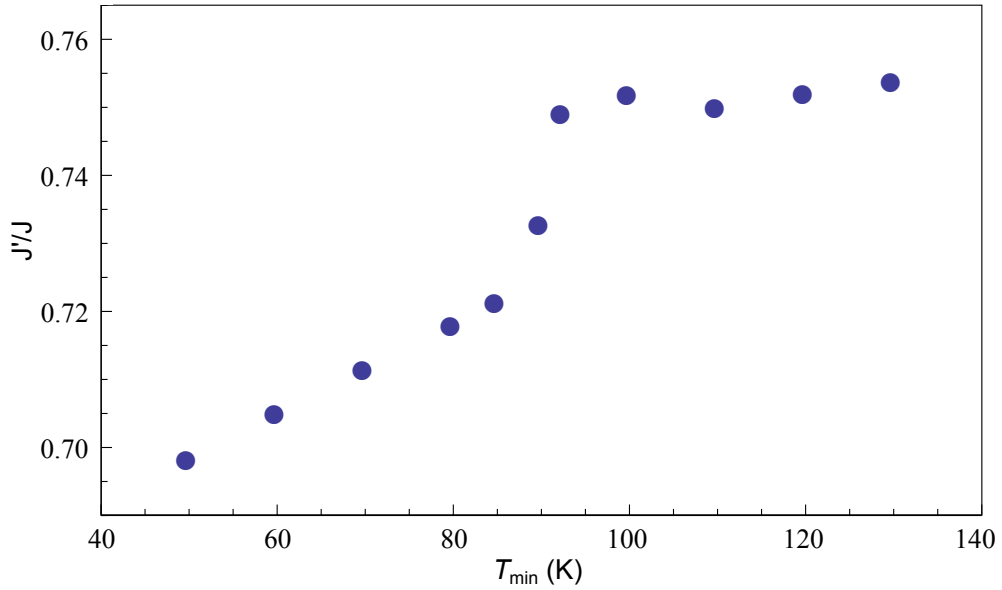

FIGURE 5.9: Best estimates of J'/J for various fitting cut-off temperatures $T_{\min}$. HTSEs are able to fit the data well down to 100 K, resulting in $J'/J = 0.75$.

came from the fact that simulated ED curves were available at much finer intervals, so that it was possible to directly obtain the J'/J with the lowest SRS value for each $T_{\min}$. In this case, the best estimate of J'/J stabilised already at $T_{\min} = 90$ K and resulted in $J'/J = 0.73$. This is consistent with the value $J'/J = 0.75$ obtained in HTSE fitting, even surprisingly so. Since our exact diagonalisation simulations contained only 16 Cu sites and completely neglected the interlayer coupling, one could have expected the two results to be more different than that. Thus we can conclude that the values obtained for $J'/J = 0.75$ and exchange couplings are quite robust and precise.

Figure 5.10 demonstrates the final HTSE and ED fits. The $J'/J = 0.75$ HTSE curve was fitted down to $T_{\min} = 100$ K and resulted in parameters $J = 79.7$ K, $g = 2.184$, $\chi_0 = -0.000066$ emu/mol.For the ED curve, the corresponding numbers are $J'/J = 0.73$, $T_{\min} = 90$ K,$J = 85.2$ K, $g = 2.167$, $\chi_0 = -0.000058$ emu/mol.

Finally, our microscopic magnetic model and its parameters can also be verified by comparing the experimental magnetisation isotherm with its counterpart obtained by diagonalising the Hamiltonian (either by exact or Lanczos diagonalisation). There are two ways how our model parameters results influence the predicted

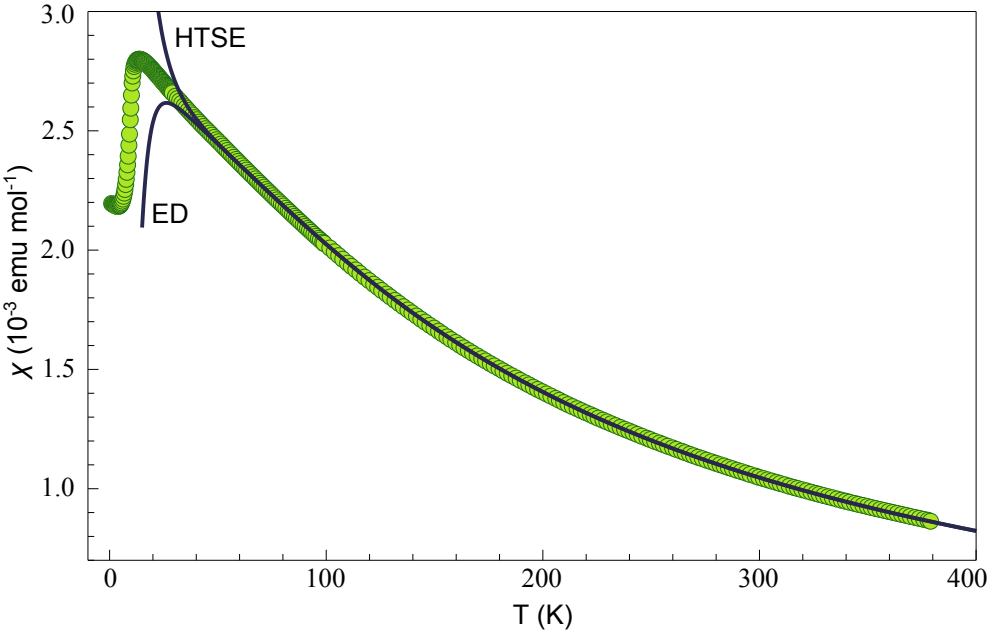

FIGURE 5.10: Final HTSE and ED fits of magnetic susceptibility.

magnetisation isotherm. The Shastry-Sutherland model Hamiltonian with $J'/J = 0.75$ that is used for diagonalisation determines the qualitative behaviour of the magnetisation curve. Secondly, the g-factor and J-value from the final HTSE fit set scales of H and M.

Figure 5.11 displays the simulated magnetisation results together with the experimental curve. Due to the finite sizes of lattices used for diagonalisation (16 sites for ED and 24 for Lanczos), results obtained from simulations look like series of jumps rather than smooth functions. As discussed in Section 4.2.1, the other consequence of finite size is that the accuracy of describing strongly frustrated systems like Cu(OH)Cl suffers, meaning that the simulated magnetisation curve may change by a fair amount when system size is increased. We can see that within the accuracy of our simulations, diagonalisation results are generally in agreement with the experimental curve.

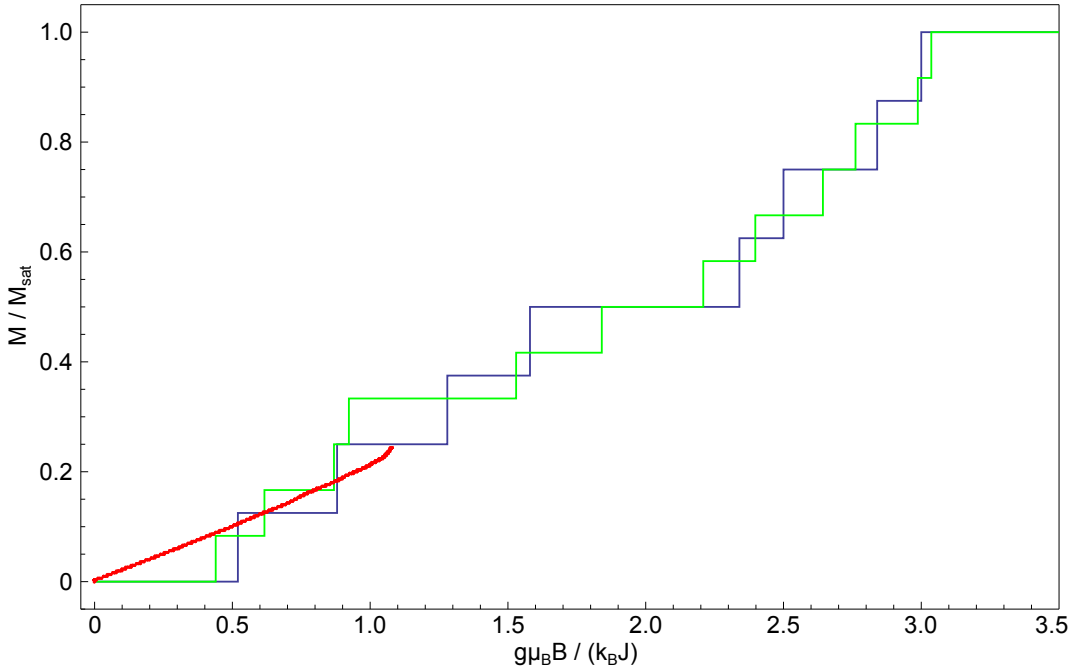

FIGURE 5.11: Magnetisation isotherms of Cu(OH)Cl: experimental (red curve), exact diagonalisation with 16 sites (blue) and Lanczos diagonalisation with 24 sites (green). The saturation magnetisation is $M_{\text{sat}} = g\mu_B/2$ (per Cu atom, as usual). HTSE fitting results $g = 2.184$ and $J = 80$ K were used to scale the experimental magnetisation curve.

6. Discussion

Even though the Shastry-Sutherland lattice is geometrically frustrated, the question still remains whether frustration plays a significant part in the physics of Cu(OH)Cl. This can be achieved by comparing our model and its parameters with known results about a very similar *non-frustrated* system, the antiferromagnetic spin-$\frac{1}{2}$ Heisenberg model on the stacked square lattice. In the latter, sites are arranged in layers of square lattice with couplings J_a, additionally each site is coupled to the previous and next layers via J_b. Since there is only one interlayer coupling per site in our model for Cu(OH)Cl, we assign $J_b = J_{\text{int}}/2 = 3J/16$. The magnitude of intralayer couplings can be characterised by $J_a = (4J' + J)/4 = (4 \cdot 0.75J + J)/4 = J$. According to previous theoretical results [26], a stacked square lattice with these values of J_a and J_b would be expected to undergo long-range ordering at $T_N/J_a \approx 0.5$, but experimental results for Cu(OH)Cl put the phase transition to a significantly lower value, $T_N/J = (11\text{ K})/(80\text{ K}) \approx 0.14$. This serious drop in the Néel ordering temperature is a clear indication of the importance of frustration in Cu(OH)Cl.

The value $J'/J = 0.75$ that we determined for Cu(OH)Cl is very close to the predicted point of quantum phase transition $J'/J = 0.765(15)$ of the Shastry-Sutherland model (Section 3.2). This makes Cu(OH)Cl a very interesting compound as it potentially enables us to learn something about the phase diagram. However, given that two simplifications were made to describe Cu(OH)Cl by a Shastry-Sutherland model, the applicability of theoretical results obtained for the basic Shastry-Sutherland model to Cu(OH)Cl needs careful consideration.

The first simplification was equating the two interdimer couplings J_1' and J_2'. According to DFT calculations, the difference between J_1' and J_2' is quite small, of the order of 10%. In Section 5.2.1, it was shown that the effect of that on magnetic susceptibility curves was small, so this difference will likely not take Cu(OH)Cl to a different region of the phase diagram. This argument is supported by a theoretical study concerning the spin-$\frac{1}{2}$ Shastry-Sutherland lattice of $(CuCl)LaNb_2O_7$ that has different (although ferromagnetic) interdimer couplings [75]. In this paper, phase diagrams of the "distorted" Shastry-Sutherland model were calculated by three methods – none of these predict that introducing a 10% difference between interdimer couplings could lead to a new phase.

A more important deviation from the basic two-dimensional Shastry-Sutherland model is the sizeable interlayer coupling J_{int}. A careful analysis of the system shows that interlayer couplings are not frustrated, meaning that they will facilitate long-range ordering of magnetic moments. This suggests that previous theoretical analyses of the Shastry-Sutherland model, in particular of the dependence of quantum phases on the ratio J'/J, cannot be straightforwardly applied to Cu(OH)Cl with high precision. Since the presence of J_{int} inclines the system towards ordering, transition to the Néel phase should occur at a lower J'/J value than in the classical Shastry-Sutherland system. In principle, an interlayer coupling of high enough magnitude might even be able to destroy the intermediate plaquette phase. The question of what exactly happens with the phases would require a thorough investigation on its own, but some insight can be gained from previous results on similar systems.

The influence of the interlayer coupling on magnetic ordering has been theoretically investigated for the case of the spin-$\frac{1}{2}$ J_1-J_2 antiferromagnetic Heisenberg model on the stacked square lattice [76]. Each layer of this 3D model consists of a square lattice of couplings J_1, to which next-nearest-neighbour couplings J_2 have been added along the diagonals of the squares. Additionally, each site is coupled to the previous and the next layer by J_{int}. The presence of diagonal J_2 couplings makes the model very strongly frustrated, which allows three phases to emerge. In case of $J_{\text{int}} = 0$, there are two long-range ordered phases at small and large J_2

and between these lies an intermediate quantum paramagnetic phase without long-range order. It was discovered that the parameter region of the intermediate phase narrows when J_{int} is increased, disappearing completely at $J_{\text{int}} \sim (0.2 - 0.3)J_1$. As the effective strength of interlayer couplings in our model for Cu(OH)Cl is about $0.25J' \approx 0.20J$, we can expect by analogy that by that value of J_{int} the intermediate phase of the Shastry-Sutherland lattice is either strongly suppressed or has disappeared at all.

Taking these considerations into account, we expect that Cu(OH)Cl (with $J'/J = 0.75$) lies in the Néel phase part of the phase diagram. Even though the transition between the Néel phase and the plaquette phase is predicted to occur at $J'/J = 0.765(15)$ for the classical Shastry-Sutherland model, the interlayer coupling present in Cu(OH)Cl should lower this boundary. In addition, we know from experiment that Cu(OH)Cl undergoes long-range ordering at 11 K, which is consistent with it being in the Néel phase part of the phase diagram.

If Cu(OH)Cl really is in the Néel phase part of the phase diagram, then there should be no plateaux in its magnetic susceptibility curve. Our current experimental results confirm that claim up to 59 T, but it is still possible that plateaux exist at higher values of magnetic field. This is what our diagonalisation results suggest – in Figure 5.11, there seems to be a plateau at half of maximum magnetisation. However, we have to keep in mind that these simulations have been carried out for a 2D model where interlayer couplings have been neglected. Therefore magnetisation simulations do not change our prediction – if Cu(OH)Cl truly is in the Néel phase part of the phase diagram, no plateaux in magnetic susceptibility should be observed even if it were measured up to higher magnetic fields. This can be verified by carrying out ultra-high-field magnetisation measurements.

Another possible source of discrepancies between our microscopic model and the reality in Cu(OH)Cl can be the fact that we used a simple Heisenberg model and completely neglected Dzyaloshinskii-Moriya (DM) interactions. Luckily, it can be roughly estimated how much they can affect our results without turning to detailed calculations. Firstly, as was discussed in Section 2.1, the strength

of Dzyaloshinskii-Moriya interactions is typically 1-2 orders of magnitude smaller than the superexchange interactions that give rise to J, J' and J_{int}. Secondly, since there can be no DM interaction between two sites if there is inversion symmetry about the centre of the line connecting the two ions, we can check whether DM interactions can have an effect at all. From the structure of Cu(OH)Cl it can be seen that DM interactions can be present in the J' coupling, but not in the J or J_{int} couplings. Taking this into account, we do not expect DM interactions to affect our microscopic magnetic model significantly.

Having established the validity of our microscopic magnetic model of Cu(OH)Cl, we can now turn our attention to comparing Cu(OH)Cl with similar systems. One useful reference compound is $SrCu_2(BO_3)_2$, as many of its properties have been well studied. In addition to that, it is worth considering Cu(OH)F – a compound that contains copper plaquette dimers connected with one another along the corners in a very similar fashion as in Cu(OH)Cl [77]. Its synthesis is more difficult, though, so there is no data about its magnetic properties. However, even just based on the structure, we expect that there are sizeable Cu-Cu exchange couplings along oxygen bridges (but there can be additional important couplings, too).

A detailed analysis of Cu(OH)F would be outside the scope of this work, but the main structural characteristics of expected couplings are given in Table 6.1. These can be compared with the corresponding parameters of Cu(OH)Cl and $SrCu_2(BO_3)_2$. It should be noted that in $SrCu_2(BO_3)_2$, the copper atoms participating in the J' coupling are not separated just by an oxygen atom, which is why the Cu-O-Cu angle is not included for that case.

It is evident from Table 6.1 that the structures of Cu(OH)Cl and Cu(OH)F are very similar. For both compounds, Cu-Cu distances and angles increase in the order $J \to J'_1 \to J'_2$, and the value of each parameter for Cu(OH)Cl is greater than that of the Cu(OH)F equivalent. Whereas having Cu sites closer together may not have any direct effect on the microscopic magnetic model because the intradimer interaction is of superexchange type, smaller Cu-O-Cu angles are expected to have a clear impact. It weakens the antiferromagnetic superexchange mechanism and

TABLE 6.1: Structural parameters of (a) Cu(OH)F [77], (b) Cu(OH)Cl [27] and (c) $SrCu_2(BO_3)_2$ [78], together with the values of exchange couplings for the latter two.

	Cu-Cu distance (Å)			Cu-O-Cu angle			Coupling value (K)	
	(a)	(b)	(c)	(a)	(b)	(c)	(b)	(c) [8]
J	2.98	3.03	2.91	97.8°	98.8°	98.5°	80	85
J'_1	3.11	3.29	5.13	103.6°	109.5°	N/A	60	54
J'_2	3.19	3.36	5.13	107.4°	114.0°	N/A	60	54

favours Hund's coupling on ligand sites, thus decreasing the values of exchange couplings by making them more ferromagnetic. Magnitudes of these changes are difficult to predict, but we can get a rough idea by looking at the Cu(OH)Cl results. There we saw the value of J drop from $\sim$ 300 K to $\sim$ 50 K when the ferromagnetic contribution was taken into account (Table 5.1). Similarly, J' decreased from $\sim$ 150 K to $\sim$ 60 K. We see that both ferro- and antiferromagnetic contributions are sizeable and a shift towards favouring ferromagnetic interactions in Cu(OH)F can really make a difference to exchange couplings, perhaps even allow the ferromagnetic component to dominate. Therefore further investigation of Cu(OH)F would be necessary to obtain even qualitative estimates of its exchange couplings.

In addition to looking for new compounds, there is another way how the phase diagram of the Shastry-Sutherland model can be explored. Applying pressure on a crystal alters its lattice parameters and coordinates of atoms and thus can change the exchange couplings between magnetic sites. Of course, at some pressure the compound may undergo a structural phase transition and require a completely different model for the description of its magnetic properties, but before that happens it is often possible to see the parameters of the original model varied. Using exactly this approach, it has been proposed that in $SrCu_2(BO_3)_2$ the J'/J ratio increases with pressure – at $P = 2.0$ GPa, the system may enter the plaquette phase of the Shastry-Sutherland model [79, 80].

In layered compounds, the effect of pressure is usually most noticeable along the direction pointing out of the plane of layers and depends very much on how exactly the layers are connected. In $SrCu_2(BO_3)_2$, Cu-containing layers are separated only by planes of Sr atoms. This is very different from Cu(OH)Cl, where layers are tied together by hydrogen bonds between H and Cl atoms. For that reason, it would be interesting to look into the effect of pressure on Cu(OH)Cl.

Finally, one can alter the exchange couplings by substituting some atoms for another element. This is not as elegant an approach as varying pressure, because doping disrupts the formation of long-range order by introducing disorder to the system. Nevertheless, it has been done for $SrCu_2(BO_3)_2$ with various results. Replacing some Sr with Al, La, Na or Y led to strong suppression of the spin gap [81]. On the other hand, the most notable effect of diluting the system by substituting some of the Cu for Mg [82] was the introduction of new excitations into the spin gap of $SrCu_2(BO_3)_2$. A similar approach in Cu(OH)Cl might be carried out by replacing Cl with F or Br (the F case was already discussed) and could potentially lead to interesting results.

7. Summary and conclusions

Cu(OH)Cl contains Cu^{2+} ions with the $3d^9$ outer shell configuration. The unpaired electrons are well localised on Cu^{2+} ions, thus giving rise to spin $S = \frac{1}{2}$ magnetic moments and making the compound paramagnetic. However, being localised does not make the magnetic moments independent, electrons influence one another by strong correlation effects. These effects are displayed in magnetic properties of the material, leaving an imprint on experimentally measurable thermodynamic quantities like magnetic susceptibility, magnetisation and specific heat. By describing the system as a Heisenberg model with pairwise exchange couplings J_{ij} between magnetic sites, its magnetic properties can be explained.

The microscopic magnetic model for Cu(OH)Cl was determined by *ab-initio* density functional theory calculations, either by constructing a Hubbard model on top of LDA band structure or by invoking DFT+U. Model parameters were refined by fitting the experimental curve of magnetic susceptibility with the help of high temperature series expansions. Correctness of the model was verified by diagonalising the Hamiltonian to simulate thermodynamic properties, and by analysing experimental curves of magnetisation and specific heat.

We found that the magnetic properties of Cu(OH)Cl can be well described by a quasi-two-dimensional spin model. Layers of Cu^{2+} ions are arranged in a distorted Shastry-Sutherland lattice (a square lattice with some extra diagonal bonds that introduce frustration to the model) and are connected by moderate interlayer exchange couplings (J_{int}). In case of Cu(OH)Cl, the extra diagonal bonds arise from nearest-neighbour couplings J within dimers of CuO_3Cl plaquettes, whereas the main square lattice is composed of next-nearest-neighbour couplings J' between

Cu^{2+} ions of different dimers. Each Cu^{2+} ion also has a single interlayer coupling J_{int} connecting it with either the previous or the next layer.

According to our simulations and fitting results, the values of exchange couplings are $J = 80$ K, $J' = 60$ K and $J_{\text{int}} = 30$ K, with the ratio $J'/J = 0.75$. This puts Cu(OH)Cl near the most interesting parameter region of the Shastry-Sutherland model, i.e. the part where quantum phase transitions occur. Based on latest simulation results in the literature [43], if the ratio J'/J is increased above 0.675, the ground state of the Shastry-Sutherland model changes from a product of dimer singlets to a plaquette state. The latter in turn is replaced by a Néel-type antiferromagnetic ground state when J'/J exceeds 0.765.

It must be noted that the theoretical results that have been obtained about the quantum phases of the Shastry-Sutherland model are not precisely applicable to Cu(OH)Cl. The first reason comes from the moderately strong interlayer coupling that favours long-range ordering and decreases the parameter range of the intermediate plaquette phase. This is why we expect Cu(OH)Cl to be in the Néel part of the phase diagram, even though the ratio $J'/J = 0.75$ we established for the compound is below the second quantum phase transition of the 2D Shastry-Sutherland model, $J'/J = 0.765$. That conclusion is supported by the λ-type anomaly at 11 K in the experimental specific heat curve, indicating a phase transition to a long-range ordered state. The second deviation from the original Shastry-Sutherland model is that in Cu(OH)Cl, the two interdimer couplings J'_1 and J'_2 are not the same by symmetry. However, our *ab-initio* results suggest that the difference is small, and exact diagonalisation simulations allowed us to conclude that physical properties of the compound are very little affected by that.

Taking all these considerations into account, we found that the Shastry-Sutherland model with interlayer couplings gives a good description of the magnetic properties of Cu(OH)Cl. The first real-world example, $SrCu_2(BO_3)_2$, received much attention because of the plateaux observed in its magnetisation curve [24]. After that, even though there have been examples of compounds with exchange couplings arranged in the Shastry-Sutherland lattice, in most cases they have only weakly

resembled the original $S = \frac{1}{2}$ antiferromagnetic Shastry-Sutherland model with various degrees of similarity. In contrast, Cu(OH)Cl not only follows closely the Shastry-Sutherland model, but is also the first example of a system in the Néel part of the phase diagram. As such a model compound, it presents a good opportunity for additional studies to further elucidate the nature of the quantum phases in Shastry-Sutherland model.

Acknowledgements

The author wishes to thank Alexander A. Tsirlin for synthesising samples of Cu(OH)Cl and measuring their physical properties, thus laying the ground for computational studies. Contributions by Jaan Oitmaa (calculations of high temperature series expansions of magnetic susceptibility) and Oleg Janson (magnetisation simulations by Lanczos diagonalisation) are also gratefully acknowledged. Most importantly, the author is indebted to his supervisors for facilitating the completion of this thesis.

Cu(OH)Cl mikroskoopiline magnetiline mudel

Taavi Pungas

Kokkuvõte

Madaladimensioonilise magnetismi uurimine on osutunud väga viljakaks valdkonnaks, eriti Cu^{2+}-ühendites. On oletatud, et kõrgtemperatuurne ülijuhtivus kupraatides on seotud nendes leiduvate CuO_2 tasandite spetsiifiliste magnetiliste omadustega [2], samuti leidub mitmeid näiteid antiferromagnetilistest Cu^{2+}- materjalidest, milles magnetilised ergastused (magnonid) moodustavad Bose-Einsteini kondensaadi [6]. Nende ja paljude teiste nähtuste uurimiseks ning magnetiliste interaktsioonide aatomskaalal paremaks mõistmiseks tuleb kasuks ainete mikroskoopiline magnetiline modelleerimine. Käesoleva töö eesmärgiks oli välja selgitada Cu(OH)Cl mikroskoopiline magnetiline mudel, kasutades selleks tihedusfunktsionaaliteooria (DFT) arvutusi ja termodünaamiliste omaduste eksperimentaalandmete sobitamist simulatsioonitulemustega.

Cu(OH)Cl sisaldab Cu^{2+} ioone, mille väline elektronkiht on $3d^9$ konfiguratsiooniga. Igal Cu^{2+} ioonil paikneb seetõttu üks paardumata elektron, mis teeb ioonist spinn-$\frac{1}{2}$ magnetmomendi ja muudab aine paramagnetiliseks. Tugevate elektronkorrelatsioonite tõttu ei ole magnetmomendid teineteisest sõltumatud. Sellise seostatuse mõjusid saab eksperimentaalselt mõõta materjali füüsikalistes omadustes, sealhulgas magnetilises läbitavuses, magnetisatsioonis ja erisoojuses. Neid omadusi aitab mikroskoopiliselt seletada Heisenbergi mudel, milles Cu^{2+} ioonid interakteeruvad omavahel paarikaupa magnetiliste sidestuste J_{ij} kaudu.

Cu(OH)Cl mikroskoopiline magnetiline mudel määrati DFT arvutuste abil, kasutades selleks esiteks arvutusliku tsoonistruktuuri sobitamist ja teiseks DFT+U meetodeid. Parameetreid täpsustati eksperimentaalandmete abil, sobitades magnetilise läbitavuse kõverat kõrge temperatuuri rittaarendustega. Mudeli kehtivust hinnati lisaks ka hamiltoniaani diagonaliseerimise teel termodünaamilisi omadusi simuleerides, samuti magnetisatsiooni ja erisoojuse mõõtmistulemusi analüüsides.

Töös leiti, et Cu(OH)Cl magnetilisi omadusi kirjeldab hästi kvaasi-kahedimensionaalne antiferromagnetiline spinnimudel. Cu^{2+} ioonid asuvad kihtidena Shastry-Sutherlandi võres, s.t. ruutvõres (sidestustega J'), millele lisanduvad mõned diagonaalsed sidestused J. Iga Cu^{2+} iooni ühendab kas eelmise või järgmise tasandiga mõõdukas kihtidevaheline sidestus J_{int}. Et diagonaalsete J-sidestuste mõju vastandub ruutvõre J'-interaktsioonidele, on mudel geomeetriliselt frustreeritud.

Simulatsioonide ja sobituste tulemusena leiti Cu(OH)Cl jaoks järgmised sidestuste väärtused: $J = 80$ K, $J' = 60$ K ja $J_{\mathrm{int}} = 30$ K. Seejuures on sidestuste suhe $J'/J = 0.75$ Shastry-Sutherlandi mudeli kõige huvitavama piirkonna lähistel, kus toimuvad kvantfaasiüleminekud. Hiljutisimate simulatsioonitulemuste kohaselt muutub J'/J suhet üle 0.675 suurendades Shastry-Sutherlandi mudeli põhiolek singlettide korrutisest plakettseisundiks [43]. Viimane asendub omakorda Néeli-tüüpi antiferromagnetilise põhiseisundiga, kui J'/J väärtus ületab 0.765.

Et Cu(OH)Cl mikroskoopiline magnetiline mudel ei ole täiuslikult kahedimensionaalne, vaid sisaldab ka kihtidevahelist sidestust J_{int}, ei saa tavalise Shastry-Sutherlandi mudeli faaside kohta leitud tulemusi otse üle võtta. J_{int} peaks soodustama magnetilist korrastust ja kitsendama plakettfaasi parameetripiirkonda. Seetõttu asub Cu(OH)Cl tõenäoliselt siiski Néeli faasi piirkonnas, hoolimata J'/J väärtusest $0.75 < 0.765$. Seda järeldust kinnitavad erisoojuse mõõtmistulemused, millest nähtuv λ-tüüpi anomaalia 11 K juures on magnetilise korrastuse moodustumise kindel tunnus.

Kõike eeltoodut arvesse võttes võime väita, et kihtidevaheliste sidestustega Shastry-Sutherlandi mudel kirjeldab hästi Cu(OH)Cl magnetilisi omadusi. Kuigi pärast esimese korraliku Shastry-Sutherlandi mudeliga materjali, $SrCu_2(BO_3)_2$ avastamist on veel seda tüüpi ühendeid leitud, on nad üsna nõrgalt algse spinn-$\frac{1}{2}$ antiferromagnetilise Shastry-Sutherlandi mudeliga sarnanenud. Seevastu Cu(OH)Cl ei ole mitte ainult hea näidis Shastry-Sutherlandi mudelist, vaid on lisaks ka esimene aine faasidiagrammi Néeli faasi piirkonnas. Selle ühendi edasised uuringud annaksid suurepärase võimaluse Shastry-Sutherlandi mudeli kvantfaaside olemuse mõistmiseks.

A. Coefficients of HTSEs

Here, the coefficients of high temperature series expansions of magnetic susceptibility are listed the way they were calculated by J. Oitmaa. These coefficients can be used to find the high-temperature part of the magnetic susceptibility curve according to the formula

$$\chi(T) = \frac{N_A \mu_B^2 g^2}{k_B T} \sum_{n=0}^{10} c_n \left(\frac{J}{4T}\right)^n .$$

	$J' = 0.60J$	$J' = 0.65J$	$J' = 0.70J$	$J' = 0.75J$	$J' = 0.80J$
	$J_{\text{int}} = 0.30J$	$J_{\text{int}} = 0.325J$	$J_{\text{int}} = 0.35J$	$J_{\text{int}} = 0.375J$	$J_{\text{int}} = 0.40J$
c_0	0.25	0.25	0.25	0.25	0.25
c_1	-0.925000000736	-0.981249999172	-1.03749999920	-1.09375000000	-1.1499999994
c_2	2.15749989298	2.45359344781	2.76437515637	3.08984375000	3.42999998166
c_3	-3.66291660223	-4.50957659031	-5.46088561071	-6.52164713550	-7.69666672292
c_4	6.53164241803	8.63842766534	11.1764349197	14.1944376612	17.7436002631
c_5	-15.0523000554	-20.9209207376	-28.4327479793	-37.8905156349	-49.6293383637
c_6	29.7043284128	44.1915413704	63.9201050904	90.2385070021	124.725489501
c_7	-39.7936191263	-66.2064431267	-105.253142167	-161.303363403	-239.788569533
c_8	63.9026605528	114.918452750	196.426419747	322.012615486	509.712847291
c_9	-197.806429587	-351.123010180	-602.971155347	-1004.08395005	-1625.57209367
c_{10}	400.247986378	762.308672326	1391.49198152	2447.29999260	4165.16153611

Bibliography

[1] J. Bednorz and K. Müller, "Possible high T_c superconductivity in the Ba-La-Cu-O system," Zeitschrift für Physik B Condensed Matter **64**, 189–193 (1986).

[2] P. W. Anderson, "The resonating valence bond state in La_2CuO_4 and superconductivity," Science **235**, 1196–1198 (1987).

[3] I. S. Jacobs, J. W. Bray, H. R. Hart, L. V. Interrante, J. S. Kasper, G. D. Watkins, D. E. Prober and J. C. Bonner, "Spin-Peierls transitions in magnetic donor-acceptor compounds of tetrathiafulvalene (TTF) with bisdithiolene metal complexes," Phys. Rev. B **14**, 3036–3051 (1976).

[4] J. W. Bray, H. R. Hart, L. V. Interrante, I. S. Jacobs, J. S. Kasper, G. D. Watkins, S. H. Wee and J. C. Bonner, "Observation of a spin-Peierls transition in a Heisenberg antiferromagnetic linear-chain system," Phys. Rev. Lett. **35**, 744–747 (1975).

[5] M. Hase, I. Terasaki and K. Uchinokura, "Observation of the spin-Peierls transition in linear Cu^{2+} (spin-1/2) chains in an inorganic compound $CuGeO_3$," Phys. Rev. Lett. **70**, 3651–3654 (1993).

[6] T. Giamarchi, C. Rüegg and O. Tchernyshyov, "Bose-Einstein condensation in magnetic insulators," Nature Physics **4**, 198–204 (2008).

[7] B. S. Shastry and B. Sutherland, "Exact ground state of a quantum mechanical antiferromagnet," Physica B+C **108**, 1069 – 1070 (1981).

[8] S. Miyahara and K. Ueda, "Theory of the orthogonal dimer Heisenberg spin model for $SrCu_2(BO_3)_2$," Journal of Physics: Condensed Matter **15**, R327 (2003).

[9] W. Heisenberg, "Mehrkörperproblem und resonanz in der quantenmechanik," Zeitschrift für Physik **38**, 411–426 (1926).

[10] S. Blundell, *Magnetism in Condensed Matter*, pp. 74–77 (Oxford University Press, Oxford, 2001).

[11] P. W. Anderson, "New approach to the theory of superexchange interactions," Phys. Rev. **115**, 2–13 (1959).

[12] P. W. Anderson, "Theory of magnetic exchange interactions: Exchange in insulators and semiconductors," Solid State Physics **14**, 99 – 214 (1963).

[13] J. Hubbard, "Electron correlations in narrow energy bands," Proceedings of the Royal Society of London. Series A. Mathematical and Physical Sciences **276**, 238–257 (1963).

[14] L. Shekhtman, O. Entin-Wohlman and A. Aharony, "Moriya's anisotropic superexchange interaction, frustration, and Dzyaloshinsky's weak ferromagnetism," Phys. Rev. Lett. **69**, 836–839 (1992).

[15] V. V. Mazurenko, S. L. Skornyakov, A. V. Kozhevnikov, F. Mila and V. I. Anisimov, "Wannier functions and exchange integrals: The example of $LiCu_2O_2$," Phys. Rev. B **75**, 224408 (2007).

[16] I. Dzyaloshinsky, "A thermodynamic theory of "weak" ferromagnetism of antiferromagnetics," Journal of Physics and Chemistry of Solids **4**, 241 – 255 (1958).

[17] T. Moriya, "Anisotropic superexchange interaction and weak ferromagnetism," Phys. Rev. **120**, 91–98 (1960).

[18] Y. C. Arango, E. Vavilova, M. Abdel-Hafiez, O. Janson, A. A. Tsirlin, H. Rosner, S.-L. Drechsler, M. Weil, G. Nénert, R. Klingeler, O. Volkova, A. Vasiliev,

V. Kataev and B. Büchner, "Magnetic properties of the low-dimensional spin-1/2 magnet α-$Cu_2As_2O_7$," Phys. Rev. B **84**, 134430 (2011).

[19] O. Janson, A. A. Tsirlin, J. Sichelschmidt, Y. Skourski, F. Weickert and H. Rosner, "Long-range superexchange in $Cu_2A_2O_7$ (A= P, As, V) as a key element of the microscopic magnetic model," Phys. Rev. B **83**, 094435 (2011).

[20] M. S. Kim and M. C. Aronson, "Heavy fermion compounds on the geometrically frustrated Shastry–Sutherland lattice," Journal of Physics: Condensed Matter **23**, 164204 (2011).

[21] S. E. Nagler, D. A. Tennant, R. A. Cowley, T. G. Perring and S. K. Satija, "Spin dynamics in the quantum antiferromagnetic chain compound $KCuF_3$," Phys. Rev. B **44**, 12361–12368 (1991).

[22] M. Azuma, Z. Hiroi, M. Takano, K. Ishida and Y. Kitaoka, "Observation of a spin gap in $SrCu_2O_3$ comprising spin-$\frac{1}{2}$ quasi-1D two-leg ladders," Phys. Rev. Lett. **73**, 3463–3466 (1994).

[23] J. S. Helton, K. Matan, M. P. Shores, E. A. Nytko, B. M. Bartlett, Y. Yoshida, Y. Takano, A. Suslov, Y. Qiu, J.-H. Chung, D. G. Nocera and Y. S. Lee, "Spin dynamics of the spin-$\frac{1}{2}$ kagome lattice antiferromagnet $ZnCu_3(OH)_6Cl_2$," Phys. Rev. Lett. **98**, 107204 (2007).

[24] H. Kageyama, K. Yoshimura, R. Stern, N. V. Mushnikov, K. Onizuka, M. Kato, K. Kosuge, C. P. Slichter, T. Goto and Y. Ueda, "Exact dimer ground state and quantized magnetization plateaus in the two-dimensional spin system $SrCu_2(BO_3)_2$," Phys. Rev. Lett. **82**, 3168–3171 (1999).

[25] N. D. Mermin and H. Wagner, "Absence of ferromagnetism or antiferromagnetism in one- or two-dimensional isotropic Heisenberg models," Phys. Rev. Lett. **17**, 1133–1136 (1966).

[26] C. Yasuda, S. Todo, K. Hukushima, F. Alet, M. Keller, M. Troyer and H. Takayama, "Néel temperature of quasi-low-dimensional Heisenberg antiferromagnets," Phys. Rev. Lett. **94**, 217201 (2005).

[27] Y. C. et al, "Synthesis and crystal structures of Cd(OH)Cl and Cu(OH)Cl and relationship to brucite type," Journal of Solid State Chemistry **151**, 308–312 (2000).

[28] S. Lebernegg, A. A. Tsirlin, O. Janson and H. Rosner, "Two energy scales of spin dimers in clinoclase $Cu_3(AsO_4)(OH)_3$," Phys. Rev. B **87**, 235117 (2013).

[29] S. Lebernegg, A. A. Tsirlin, O. Janson and H. Rosner, "Spin gap in malachite $Cu_2(OH)_2CO_3$ and its evolution under pressure," Phys. Rev. B **88**, 224406 (2013).

[30] K. Onizuka, H. Kageyama, Y. Narumi, K. Kindo, Y. Ueda and T. Goto, "$\frac{1}{3}$ magnetization plateau in $SrCu_2(BO_3)_2$ - stripe order of excited triplets," Journal of the Physical Society of Japan **69**, 1016–1018 (2000).

[31] Y. H. Matsuda, N. Abe, S. Takeyama, H. Kageyama, P. Corboz, A. Honecker, S. R. Manmana, G. R. Foltin, K. P. Schmidt and F. Mila, "Magnetization of $SrCu_2(BO_3)_2$ in ultrahigh magnetic fields up to 118 T," Phys. Rev. Lett. **111**, 137204 (2013).

[32] C. Tassel, J. Kang, C. Lee, O. Hernandez, Y. Qiu, W. Paulus, E. Collet, B. Lake, T. Guidi, M.-H. Whangbo, C. Ritter, H. Kageyama and S.-H. Lee, "Ferromagnetically coupled Shastry-Sutherland quantum spin singlets in $(CuCl)LaNb_2O_7$," Phys. Rev. Lett. **105**, 167205 (2010).

[33] T. Ozawa, T. Taniguchi, Y. Kawaji, S. Mizusaki, Y. Nagata, Y. Noro, H. Samata, H. Mitamura and S. Takayanagi, "Magnetization and specific heat measurement of the Shastry–Sutherland lattice compounds: Ln_2BaPdO_5 (Ln = La, Pr, Nd, Sm, Eu, Gd, Dy, Ho)," Journal of Alloys and Compounds **448**, 96 – 103 (2008).

[34] K. Siemensmeyer, E. Wulf, H.-J. Mikeska, K. Flachbart, S. Gabáni, S. Mat'aš, P. Priputen, A. Efdokimova and N. Shitsevalova, "Fractional magnetization plateaus and magnetic order in the Shastry-Sutherland magnet TmB_4," Phys. Rev. Lett. **101**, 177201 (2008).

[35] S. Yoshii, T. Yamamoto, M. Hagiwara, T. Takeuchi, A. Shigekawa, S. Michimura, F. Iga, T. Takabatake and K. Kindo, "High-field magnetization of TbB_4," Journal of Magnetism and Magnetic Materials **310**, 1282 – 1284 (2007). Proceedings of the 17th International Conference on Magnetism The International Conference on Magnetism.

[36] M. S. Kim and M. C. Aronson, "Spin liquids and antiferromagnetic order in the Shastry-Sutherland-lattice compound Yb_2Pt_2Pb," Phys. Rev. Lett. **110**, 017201 (2013).

[37] N. Ashcroft and N. Mermin, *Solid State Physics*, pp. 712–713 (Saunders College, Philadelphia, 1976).

[38] M. A. Ruderman and C. Kittel, "Indirect exchange coupling of nuclear magnetic moments by conduction electrons," Phys. Rev. **96**, 99–102 (1954).

[39] T. Kasuya, "A theory of metallic ferro- and antiferromagnetism on Zener's model," Progress of Theoretical Physics **16**, 45–57 (1956).

[40] K. Yosida, "Magnetic properties of Cu-Mn alloys," Phys. Rev. **106**, 893–898 (1957).

[41] S. Miyahara and K. Ueda, "Exact dimer ground state of the two dimensional Heisenberg spin system $SrCu_2(BO_3)_2$," Phys. Rev. Lett. **82**, 3701–3704 (1999).

[42] A. Koga and N. Kawakami, "Quantum phase transitions in the Shastry-Sutherland model for $SrCu_2(BO_3)_2$," Phys. Rev. Lett. **84**, 4461–4464 (2000).

[43] P. Corboz and F. Mila, "Tensor network study of the Shastry-Sutherland model in zero magnetic field," Phys. Rev. B **87**, 115144 (2013).

[44] W. Zheng, J. Oitmaa and C. J. Hamer, "Phase diagram of the Shastry-Sutherland antiferromagnet," Phys. Rev. B **65**, 014408 (2001).

[45] M. Albrecht and F. Mila, "First-order transition between magnetic order and valence bond order in a 2D frustrated Heisenberg model," EPL (Europhysics Letters) **34**, 145 (1996).

[46] E. Manousakis, "The spin-$\frac{1}{2}$ Heisenberg antiferromagnet on a square lattice and its application to the cuprous oxides," Rev. Mod. Phys. **63**, 1–62 (1991).

[47] N. Ashcroft and N. Mermin, *Solid State Physics*, pp. 655–656 (Saunders College, Philadelphia, 1976).

[48] N. Ashcroft and N. Mermin, *Solid State Physics*, p. 718 (Saunders College, Philadelphia, 1976).

[49] M. D. Johannes, J. Richter, S.-L. Drechsler and H. Rosner, "$Sr_2Cu(PO_4)_2$: A real material realization of the one-dimensional nearest neighbor Heisenberg chain," Phys. Rev. B **74**, 174435 (2006).

[50] S. Lebernegg, A. A. Tsirlin, O. Janson and H. Rosner, "Nearly compensated exchange in the dimer compound callaghanite $Cu_2Mg_2(CO_3)(OH)_6 \cdot 2H2O$," Phys. Rev. B **89**, 165127 (2014).

[51] N. Ashcroft and N. Mermin, *Solid State Physics*, p. 711 (Saunders College, Philadelphia, 1976).

[52] M. E. Fisher, "Relation between the specific heat and susceptibility of an antiferromagnet," Philosophical Magazine **7**, 1731–1743 (1962).

[53] N. Ashcroft and N. Mermin, *Solid State Physics*, p. 457 (Saunders College, Philadelphia, 1976).

[54] P. Hohenberg and W. Kohn, "Inhomogeneous electron gas," Phys. Rev. **136**, B864–B871 (1964).

[55] E. Engel and R. M. Dreizler, *Density Functional Theory: An Advanced Course*, pp. 57–69 (Springer, Heidelberg, 2011).

[56] E. Engel and R. M. Dreizler, *Density Functional Theory: An Advanced Course*, pp. 129–142 (Springer, Heidelberg, 2011).

[57] E. Engel and R. M. Dreizler, *Density Functional Theory: An Advanced Course*, pp. 142–145 (Springer, Heidelberg, 2011).

[58] E. Engel and R. M. Dreizler, *Density Functional Theory: An Advanced Course*, pp. 191–192 (Springer, Heidelberg, 2011).

[59] E. Engel and R. M. Dreizler, *Density Functional Theory: An Advanced Course*, pp. 169–200 (Springer, Heidelberg, 2011).

[60] J. P. Perdew, K. Burke and M. Ernzerhof, "Generalized gradient approximation made simple," Phys. Rev. Lett. **77**, 3865–3868 (1996).

[61] K. Koepernik and H. Eschrig, "Full-potential nonorthogonal local-orbital minimum-basis band-structure scheme," Phys. Rev. B **59**, 1743–1757 (1999).

[62] J. P. Perdew and Y. Wang, "Accurate and simple analytic representation of the electron-gas correlation energy," Phys. Rev. B **45**, 13244–13249 (1992).

[63] G. H. Wannier, "The structure of electronic excitation levels in insulating crystals," Phys. Rev. **52**, 191–197 (1937).

[64] A. A. Tsirlin, A. Möller, B. Lorenz, Y. Skourski and H. Rosner, "Superposition of ferromagnetic and antiferromagnetic spin chains in the quantum magnet $BaAg_2Cu[VO_4]_2$," Phys. Rev. B **85**, 014401 (2012).

[65] A. A. Tsirlin, O. Janson and H. Rosner, "β-$Cu_2V_2O_7$: A spin-$\frac{1}{2}$ honeycomb lattice system," Phys. Rev. B **82**, 144416 (2010).

[66] E. Engel and R. M. Dreizler, *Density Functional Theory: An Advanced Course*, pp. 211–217 (Springer, Heidelberg, 2011).

[67] J. Wojtkiewicz, "Quantum Monte Carlo scheme for frustrated Heisenberg antiferromagnets," Phys. Rev. B **75**, 174421 (2007).

[68] R. M. Noack and S. R. Manmana, "Diagonalization- and numerical renormalization-group-based methods for interacting quantum systems," AIP Conference Proceedings **789**, 93–163 (2005).

[69] J. K. Cullum and R. A. Willoughby, *Lanczos Algorithms for Large Symmetric Eigenvalue Computations: Vol. 1: Theory*, vol. 41.

[70] F. Alet, P. Dayal, A. Grzesik, A. Honecker, M. Körner, A. Läuchli, S. R. Manmana, I. P. McCulloch, F. Michel, R. M. Noack, G. Schmid, U. Schollwöck, F. Stöckli, S. Todo, S. Trebst, M. Troyer, P. Werner and S. Wessel, "The ALPS project: Open source software for strongly correlated systems," Journal of the Physical Society of Japan **74**, 30–35 (2005).

[71] J. Oitmaa, C. Hamer and W. Zheng, *Series expansion methods for strongly interacting lattice models*, pp. 150–178 (Cambridge University Press, Cambridge, 2006).

[72] J. Oitmaa, C. Hamer and W. Zheng, *Series expansion methods for strongly interacting lattice models*, pp. 20–21 (Cambridge University Press, Cambridge, 2006).

[73] N. Ashcroft and N. Mermin, *Solid State Physics*, pp. 648–649 (Saunders College, Philadelphia, 1976).

[74] S. Blundell, *Magnetism in Condensed Matter*, pp. 45–47 (Oxford University Press, Oxford, 2001).

[75] S. Furukawa, T. Dodds and Y. B. Kim, "Ferromagnetically coupled dimers on the distorted Shastry-Sutherland lattice: Application to (CuCl)$LaNb_2O_7$," Phys. Rev. B **84**, 054432 (2011).

[76] D. Schmalfuß, R. Darradi, J. Richter, J. Schulenburg and D. Ihle, "Quantum J_1-J_2 antiferromagnet on a stacked square lattice: Influence of the interlayer coupling on the ground-state magnetic ordering," Phys. Rev. Lett. **97**, 157201 (2006).

[77] G. Giester and E. Libowitzky, "Crystal structures and Raman spectra of Cu(OH)F and $Cu_3(OH)_2F_4$," Zeitschrift für Kristallographie **218**, 351–356 (2003).

[78] R. W. Smith and D. A. Keszler, "Synthesis, structure, and properties of the orthoborate $SrCu_2(BO_3)_2$," Journal of Solid State Chemistry **93**, 430 – 435 (1991).

[79] T. Waki, K. Arai, M. Takigawa, Y. Saiga, Y. Uwatoko, H. Kageyama and Y. Ueda, "A novel ordered phase in $SrCu_2(BO_3)_2$ under high pressure," Journal of the Physical Society of Japan **76**, 073710 (2007).

[80] S. Haravifard, A. Banerjee, J. C. Lang, G. Srajer, D. M. Silevitch, B. D. Gaulin, H. A. Dabkowska and T. F. Rosenbaum, "Continuous and discontinuous quantum phase transitions in a model two-dimensional magnet," Proceedings of the National Academy of Sciences **109**, 2286–2289 (2012).

[81] G. T. Liu, J. L. Luo, N. L. Wang, X. N. Jing, D. Jin, T. Xiang and Z. H. Wu, "Doping effects on the two-dimensional spin dimer compound $SrCu_2(BO_3)_2$," Phys. Rev. B **71**, 014441 (2005).

[82] S. Haravifard, S. R. Dunsiger, S. El Shawish, B. D. Gaulin, H. A. Dabkowska, M. T. F. Telling, T. G. Perring and J. Bonča, "In-gap spin excitations and finite triplet lifetimes in the dilute singlet ground state system $SrCu_{2-x}Mg_x(BO_3)_2$," Phys. Rev. Lett. **97**, 247206 (2006).

Lihtlitsents lõputöö reprodutseerimiseks ja lõputöö üldsusele kättesaadavaks tegemiseks

Mina, Taavi Pungas,

1. annan Tartu Ülikoolile tasuta loa (lihtlitsentsi) enda loodud teose

"The microscopic magnetic model of Cu(OH)Cl"

mille juhendajad on Alexander A. Tsirlin ja Taavi Vaikjärv,

1.1. reprodutseerimiseks säilitamise ja üldsusele kättesaadavaks tegemise eesmärgil, sealhulgas digitaalarhiivi DSpace-is lisamise eesmärgil kuni autoriõiguse kehtivuse tähtaja lõppemiseni;
1.2. üldsusele kättesaadavaks tegemiseks Tartu Ülikooli veebikeskkonna kaudu, sealhulgas digitaalarhiivi DSpace´i kaudu kuni autoriõiguse kehtivuse tähtaja lõppemiseni.

2. olen teadlik, et punktis 1 nimetatud õigused jäävad alles ka autorile.

3. kinnitan, et lihtlitsentsi andmisega ei rikuta teiste isikute intellektuaalomandi ega isikuandmete kaitse seadusest tulenevaid õigusi.

Tartus, 28.05.2014